A doctoral thesis

Study on Hydrogen Isotope Separation using Fuel Cell and Electrolysis with Polymer Electrolyte Membrane

固体高分子膜を用いた燃料電池と水電解による水素同位体分離の研究

February, 2024

Hokkaido University

Faculty of Engineering

Division of Materials Science and Engineering

北海道大学大学院 工学院 材料科学専攻

Koichiro FURUSAWA

古澤 宏一朗

Contents

Chapter 1:

General Introduction

1.1 Applications of hydrogen isotopes

Hydrogen isotopes are hydrogen (H), deuterium (D), and tritium, (T). These isotopes differ in mass number. Hydrogen has one proton, deuterium has one proton and one neutron, and tritium has one proton and two neutrons. These differences of mass result in different physical properties, such as boiling point. As a natural abundance ratio, hydrogen is 99.985% and deuterium is 0.015%, respectively.

Hydrogen is being used to reduce CO_2 emissions and as a substitute for fossil fuels to prevent global warming. In the future, grid power will need to stabilize for fluctuations in renewable energy sources such as solar and wind power generation. So that reason, hydrogen will be produced in electrolyzers using surplus electricity from variable power generation. The hydrogen produced is used as electricity and heat using fuel cells and combustors. Regarding grid connection of renewable energy, hydrogen production and utilization, the US Department of Energy has established the concept of H2@scale [1].

One application of deuterium is the use of surface treatment on semiconductors. It is known that the durability improves to replace the deuterium instead of hydrogen silicon end groups on the surface of semiconductors [2]. Therefore, it is used in some parts of the semiconductor manufacturing process.

Next, I explain the use of deuterium in pharmaceuticals. By replacing hydrogen atoms in the structure of drug with deuterium, the efficacy of the drug changes. This is because the reactivity of the drug is reduced due to the effect of deuterium's stability, and the time until metabolic decomposition is lengthened. In 2017, the FDA-certified drug deutetrabenazine (brand name Austedo) was sold as a drug using deuterium [3].

Recently, application of optical materials has also been attracting attention. For example, the replacement of hydrogen atoms with deuterium is considered as a material

for organic EL panels. This replacement can improve luminous efficiency and reduce the amount of heat generated. This can improve energy conversion efficiency and durability [4]. It has also been reported that optical loss can be reduced by using deuterated polymers in the central core as an application for optical fiber [5]. In the field of basic research, deuterated compounds have been synthesized and used to study reaction mechanisms using the difference in physical behavior between deuterated compounds and hydrogen atoms [6].

Deuterium becomes heavy water which is an oxide of deuterium. This heavy water is used as a moderator in heavy water reactors. Heavy water reactors use natural uranium as fuel, and heavy water is the most commonly used of the three moderators that enable the chain reaction of fission. The advantage of heavy water reactors is that they do not depend on a source of enriched uranium and are currently used in India, Canada, South Korea, and other countries [7].

Tritium is expected to be used in future fusion reactor. The reaction in fusion reactor is called the DT reaction and is shown in Equation (1.1). The reaction of deuterium and tritium at high temperature and high pressure produce helium-4, neutrons, and a huge amount of thermal energy. By reacting the neutrons to beryllium and lithium at the bracket inside the fusion reactor, the reactions of Equations (1.2) and (1.3) can occur. This makes it possible to breed tritium. Tritium increase quantity in after fusion reaction. Tritium from external sources is needed as the initial fuel [8].

$$D + T \rightarrow {}^{4}He + n + 17.5MeV \tag{1.1}$$

$$^{9}Be + n \rightarrow {}^{8}Be + 2n \tag{1.2}$$

$$^{6}Li + n \rightarrow {}^{4}He + T \quad (1.3)$$

The technology to separate tritium as a fusion reactor is applicable in three places [9]. One is the fuel system, which collects tritium in the gas emitted from the fusion reactor. The system makes it to adjust a concentration at which fusion can do and re-injects into fusion reactor.

Second, the system removes tritium from the cooling water. Fusion reactor has the coolant which cools the bracket of the fusion reactor, tritium inside the bracket passes through the bracket and migrates into the cooling water. Third, fusion reactor is needed to recover the tritium which are contained in the exhaust and generated inside the building. A ventilation system is installed to prevent leakage from the fusion reactor to the outside environment. The exhaust air from the building is passed through a combustor to oxidize the tritium and recover it as oxide.

1.2 The methods of hydrogen isotope separation

In general, an optimum isotope separation depends on the atomic weight of the atom. Therefore, the method varies depending on the element to be separated. For example, the method of isotope separation of uranium are used the gas diffusion and gas centrifugation methods [10]. For hydrogen isotope separation, the common methods are gas phase adsorption and cold distillation, electrolysis, and water-hydrogen chemical exchange. Other methods are a combination of these methods.

Gas-phase adsorption is a method of separation based on differences in the physical adsorption of hydrogen isotopes on zeolites at cryogenic temperatures [11]. Cryogenic distillation is a method of separation by distillation based on the difference in boiling points at cryogenic temperatures [12]. The water-hydrogen chemical exchange method is shown in Equations (1.4) and (1.5) for deuterium and light hydrogen.

The reaction in Equation (1.4) is called Vapor Phase Chemical Exchange (VPCE). This is the reaction between water vapor and HD on a Pt catalyst. This reaction is an equilibrium reaction in which D is transferred to the oxide side. The equilibrium constant is approximately 3~4. Next, the reaction in Equation (1.5) is called Liquid Phase Chemical Exchange (LPCE). This is an equilibrium reaction in which D moves to the liquid side when liquid water is present in the reaction field. These methods can increase the separation factor by continuous transfer of D to the liquid side. First D_2(gas) becomes HDO(gas), and then the flow of HDO(gas) becomes HDO(l).

$$D_2(gas) + 2H_2O(gas) \leftrightarrows 2HDO(gas) + H_2(gas) \quad (1.4)$$

$$HDO(gas) + H_2O(l) \leftrightarrows H_2O(gas) + HDO(l) \quad (1.5)$$

Next, the electrolysis method is explained. The electrolysis method uses the difference in reaction rates between hydrogen and deuterium in the electrolysis of water. Mass number is heavier , then it slows down the electrode reaction rate from ion to gas [13]. By electrolyzing raw materials containing hydrogen in an electrolysis, deuterium is concentrated in the raw materials. Because hydrogen is more easily gasified than deuterium. The electrolysis process in isotope separation began in 1933 when G.N. Lewis et al. continuously electrolyzed water in electrolysis tanks to obtain small amounts of heavy water. And this method is still used industrially today.

The CECE method is a combination of this electrolysis method and the water-hydrogen chemical exchange method. The CECE method stands for Combined Electrolysis and Catalytic Exchange (CECE). In this method, gas generated in the electrolyzer is passed through a column filled with catalysts. Isotope-free water flows upstream of the column. And then the water-hydrogen chemical exchange method of Equations (1.4) and (1.5) is performed inside the column by counter-current flow to separate isotopes. Thereby it is improved the separation factor [14]. This method is actually used in deuterium reactors [15] and is also employed in ITER, an international fusion reactor [16].

A summary of energy consumption and separation factors for different technologies in heavy water production is shown in Figure 1.1 [17]. The ideal technology for heavy water production is one that consumes less energy and has a high separation factor. The separation factor of the electrolyzer is 10, which is high compared to other technologies, but the energy consumption is 1000 GJ kg-1, which is huge. Similarly, the

CECE method uses water electrolysis, which requires an enormous amount of energy.

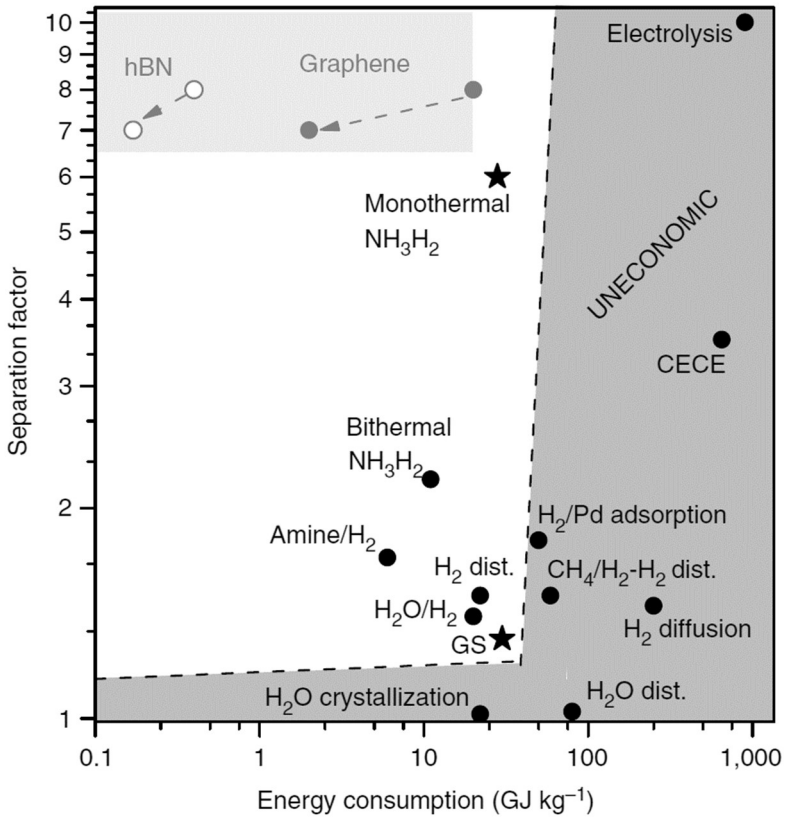

Figure1.1 Comparison of the electrochemical pumping with other technologies available for heavy-water production (Scalable and efficient separation of hydrogen isotopes using graphene-based electrochemical pumping, Lozada-Hidalgo, M; Zhang, S; et al., NATURE COMMUNICATIONS Copyright©(2017)

1.3 CEFC method

The electrolysis method is issued by the enormous amount of electricity consumed to gasify raw material. Therefore, it is necessary to explore a new electrolysis method with low power consumption. To solve this problem, this study proposes an innovative electrolytic recombination method that combines the electrolysis method with a fuel cell. The concept is shown in Figure 1.2.

The hydrogen and oxygen gases generated in the electrolyzer were previously discarded. But these gases are used to generate electricity in the fuel cell due to recover electrical energy. Water containing hydrogen isotopes produced by the fuel cell is returned to the electrolyzer. And gas of hydrogen isotopes have been removed is released into the atmosphere. In consideration of the enrichment reaction in the fuel cell, there is a possibility that hydrogen isotope separation can be achieved with even higher efficiency. As shown in Figure 1.2, this process can be carried out in a continuous cascade to recover hydrogen isotopes from the raw material. Thermodynamically, CEFC method can be separated without using much electrical energy other than ohmic loss due to the electrolyte's electrical resistance. The collected concentrated liquid is stored in a tank, and the cascade can be repeated to achieve highly concentrated separation. With the current growth of fuel cells for automobiles, the polymer electrolyte fuel cells have very high-power generation performance. In addition, they are designed to be very compact because they need to be installed in the limited space of an automobile. From the viewpoint of material circulation, automotive fuel cells are designed so that hydrogen, air, and liquid water produced by the fuel cell reaction can be discharged. Therefore, there is a possibility that the fuel cell currently in use could be converted to the industrial enrichment process shown in Figure 1.2 to make the plant more compact.

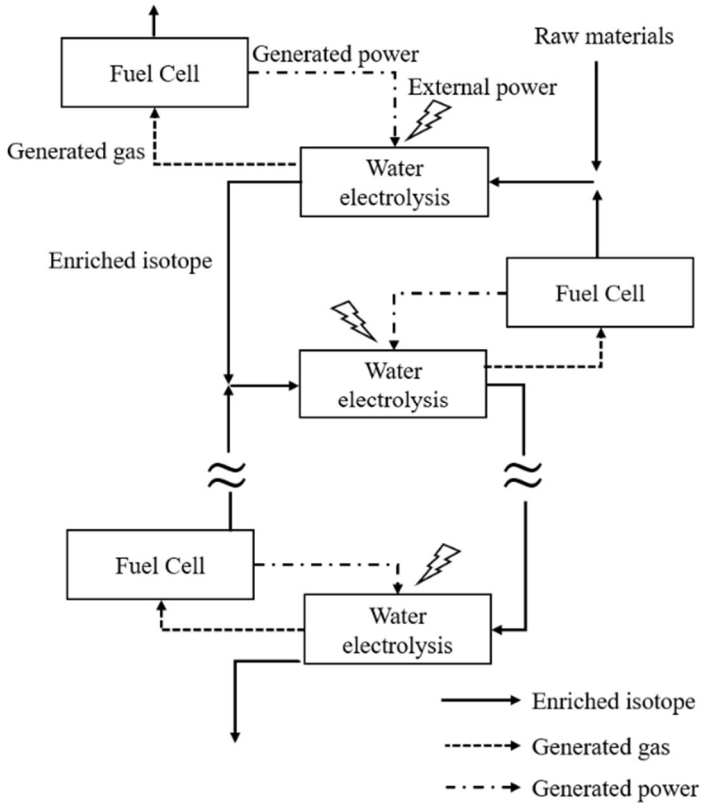

Figure1.2 Schematic diagram of the CEFC method

1.3.1 Polymer electrolyte fuel cell

The structure of a polymer electrolyte fuel cell is explained below. Figure 1.3 shows the schematic structure of a fuel cell. It consists of a separator that forms the gas and coolant channels, a gas diffusion layer for gas diffusion and discharge of product water, a catalyst layer for catalytic reaction, and a proton exchange membrane (PEM). The catalyst layer consists of highly dispersed platinum nanoparticles of several nm in size supported on a carbon substrate of several tens nm in specific surface area.

The chemical reaction in a fuel cell is shown in Equation (1.6). First, hydrogen supplied to the anode electrode is split into protons (H+) and electrons on the catalyst. And the protons move through the electrolyte membrane to the cathode electrode. At the cathode electrode, the supplied oxygen combines with the electrons from the anode electrode and the protons from the electrolyte membrane to produce water. The cathode electrocatalyst has an important role in fuel cell performance. Because electromotive force is generated by the reaction of oxygen on the cathode catalyst.

$$H_2 + 1/2\ O_2 \rightarrow H_2O \tag{1.6}$$

Research on polymer electrolyte fuel cells has been conducted since the 1990s to develop fuel cells for fuel cell vehicles and stationary power sources. Initially, the cost and size of fuel cells made it difficult to apply fuel cell vehicles. With the progress of research and development, the cost was reduced and the size became more compact. This led to the launch of fuel cell vehicles in the 2000s. Toward reduce the cost of fuel cells, research is being conducted to reduce the amount of platinum catalyst used in the

catalyst layer [18].

In addition, the size of fuel cells has been greatly reduced through technologies such as thinner electrolyte membranes and reduced thickness of separator structures. And the output power of fuel cell cells can be increased by high current density of the fuel cell. As a result, the number of fuel cell cells can be reduced, contributing to more compact fuel cell stacks.

Mass production of fuel cell vehicles has gradually begun in earnest since the 2010s, and fuel cell mass production plants are being built. Therefore, as the number of fuel cells manufactured increases, the unit cost of manufacturing fuel cells decreases, and the price of fuel cells is expected to decrease in the future [19].

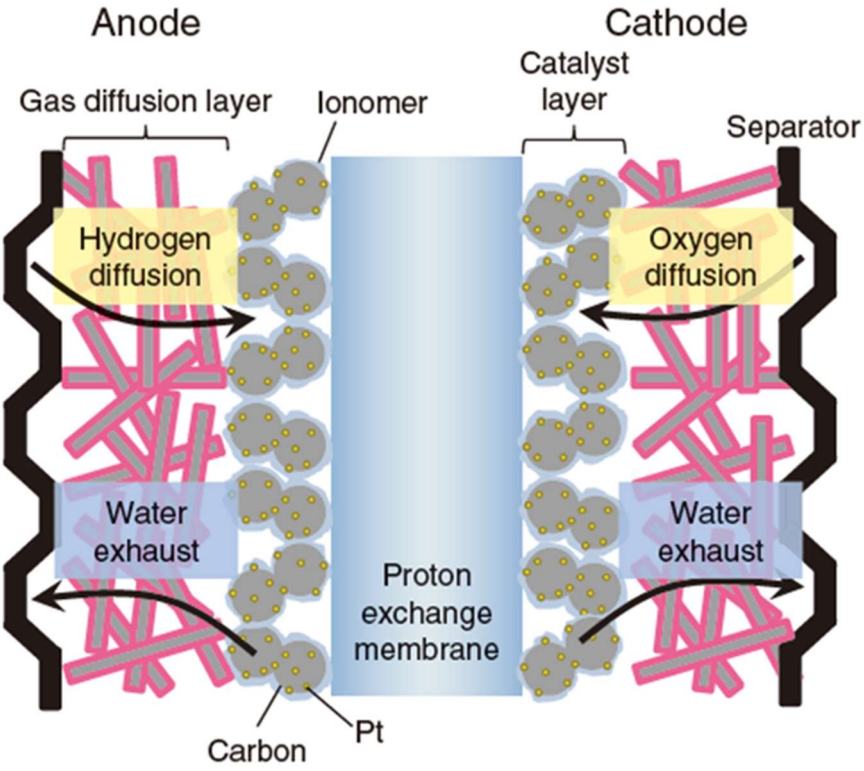

Figure 1.3 Schematic of polymer electrolyte fuel cell

1.3.2 Proton exchange membrane water electrolysis

Proton exchange membrane water electrolysis is a device used to electrolyze water to produce hydrogen and oxygen. Solid polymer is used as the electrolyte membrane in the electrolysis cell. There are electrodes at both ends of this electrolyte membrane. The electrodes are generally platinum for the cathode and iridium for the anode. Water as raw material is supplied to the anode. The water molecules are then decomposed into oxygen and protons, as shown in Equation (1.7). The protons produced pass through the electrolyte membrane and move to the cathode. At the cathode, as shown in Equation (1.8), the protons passed through the electrolyte membrane combine with electrons to produce hydrogen. Oxygen and unreacted water are discharged at the anode and hydrogen at the cathode.

$$2H_2O \rightarrow O_2 + 4H^+ + 4e^- \quad (1.7)$$

$$2H^+ + 2e^- \rightarrow H_2 \quad (1.8)$$

Compared to conventional alkaline water electrolysis, solid polymer water electrolysis has a cleaner solution, higher reaction efficiency, and produces high-purity hydrogen gas [20]. However, the cost of a solid polymer electrolyzer is considered to be higher than that of alkaline water electrolysis. Because it requires special components such as an expensive polymer membrane, porous electrodes, and current collector. Alkaline water electrolysis is used industrially because alkaline water electrolysis does not use precious metals as catalysts and is easier to scale up.

However, future cost projections predict that solid polymer type water electrolysis will be close to alkaline water electrolysis [21].

In alkaline water electrolysis, electrolytic materials are used to make the solution alkaline, which is difficult to process, so the solid polymer electrolysis is used in water electrolysis for hydrogen isotopes.

1.4 Conventional research and positioning of this study

Hydrogen isotope separation using fuel cell has been researched in terms of the different materials used in the fuel cell and the effects of power generation [22]. Separation performance in LPCE is also being researched on Pt/C and PTFE catalysts used in fuel cell [23]. A study by A. Pozio et al. used a PEFC with Pt-Ru catalyst to separate deuterium and hydrogen [24]. At that time, the analysis was performed by electrochemical impedance (EIS) and IR. By measuring with electrochemical impedance, the influence of details about the reaction resistance inside the fuel cell is investigated. This analysis showed that the isotope separation efficiency depended on current density, with a maximum separation factor at a current density of 100 mA/cm^{-1}. This is attributed to the advantage of deuterium oxidation rather than hydrogen oxidation. However, since deuterium ions move more slowly than protons inside the electrolyte membrane, the formation of heavy water is limited and the separation factor drops to a constant value as the current density increases. This research investigates the effect of reaction rate, gas concentration and residence time on the separation process.

In conventional research, main objective was to separate the effects of different PEFC materials and power generation. Therefore, the effects of humidification supplied to the PEFC and water generated inside the PEFC have not been researched. In addition, although the analysis is based on power generation, the effect of the water-hydrogen chemical exchange method inside the fuel cell has not been investigated. Since water is generated inside the fuel cell during power generation, the effect of water inside the fuel cell is considered to occur even without humidifying the inlet gas of the fuel cell. Therefore, it is necessary to investigate how the amount of supplied water and produced water affect isotope separation. In this research, the effect of water supplied to the fuel

cell was investigated on the separation. The effects of water vapor and liquid water inside the fuel cell were also investigated.

1.5 Purpose of this research

In order to put the CEFC method into practical use, it is necessary to determine the basic configuration of the system. In particular, the humidification configuration of the system must be determined because the humidification of the gas supplied in the fuel cell is critical to the performance and degradation. The electrolyte membrane contains water, it supports the movement of protons inside the electrolyte membrane [25]. Water is also transferred when protons are transferred from the anode to the cathode. For that reason, water must be supplied to the anode electrode in order for the fuel cell to generate electricity. However, the system configuration of fuel cell vehicles makes it difficult from a cost and hydrogen safety perspective to supply water to the anode. Then humidification is applied to the gas supplied to the cathode. For cathode humidification, a humidifier is used to circulate water from the cathode outlet to the inlet. Toyota MIRAI does not use a humidifier, but instead uses a configuration that returns water from the anode outlet to the anode inlet by optimally controlling. These controlling are hydrogen circulation and setpoint of pressure and flow rate [26]. And fuel cell has the internal humidification structure.

In order to construct a CEFC method system, it is important to understand in advance the effects of humidification of the supplied gas, the locations where humidification is required, the gas-liquid ratio of the supplied gases inside the fuel cell, and the effects of liquid water. Therefore, this study was conducted to analyze these effects. Since platinum is used in the fuel cell, we considered that the conventional method of water-hydrogen chemical exchange might be occurring inside the fuel cell. Experiments were conducted to separate the effects of the water-hydrogen chemical exchange from the separation caused by the fuel cell reaction. Next, the water-hydrogen

chemical exchange method involves separation by isotope exchange between gases (VPCE) and isotope separation between gas and liquid water (LPCE). Therefore, the effect of generating liquid water inside the fuel cell on the separation was confirmed.

In Chapter 2, hydrogen isotopes using fuel cells is confirmed each effects of water vapor, oxygen, and power generation. And the separation factor is measured for each effect. During the hydrogen isotope separation process, the mass balance of deuterium is measured to determine if the separation is correct. And we investigated the distribution of deuterium.

In Chapter 3, the effect of humidification in the fuel cell is confirmed. This examination confirm how the separation coefficient is affected by the difference in the amount of water vapor supplied and the vapor-liquid ratio inside the fuel cell. And the equilibrium conversion is calculated using equilibrium constants, and the calculated values are compared with experimental values.

In Chapter 4, we focused on the electrolyzer part and obtained the relationship between the concentration of deuterium and the electrolysis consumption rate during the batch type heavy water concentration. In addition, the deuterium concentration process is calculated from the mass balance for the established calculation method for the future CEFC method.

We believe that these experiments and studies will provide guidelines for the design. And development of system configurations in CEFC method will be useful. This study will be profit commercialization of the CEFC method for future.

References

[1] B. Pivovar, N. Rustagi, S. Satyapal, Electrochem. Soc. Interface, **27**, 47 (2018).

[2] J. W. Lyding, K, Hess, I. C. Kizilyalli, Appl. Phys. Lett., **68**, 252 (1996).

[3] F. Schneider, D. Stamler, M. Bradbury, P. S. Loupe, E. Hellriegel, D. S. Cox, J. M. Savola, M. F. Gordon, L. R. Guilatt, L, Clin Pharmacol Drug Dev., **10**, 647 (2021).

[4] H. Tsuji, C. Mitsui, E. Nakamura, Chem. Commun., **50**, 14870 (2014).

[5] N. Zhao, W. Li, J. Li, G. Zhou, J. Li, J. Lightwave Technol., **37**, 3021 (2019).

[6] X. Yang, H. Ben, A. J. Ragauskas, Asian J. Org. Chem., **10**, 2473 (2021).

[7] S. S. Bajaj, A. R. Gore, Nucl. Eng. Des., **236**, 701 (2006).

[8] R. J. Pearson, A. B. Antoniazzi, W. J. Nuttall, Fusion Eng. Des., **136**, 1140 (2018).

[9] M. Glugla, A. Antipenkov, S. Beloglazov, C. C. Nlchols, I. R. Cristescu, I. Cristescu, C. Day, L. Doerr, J. P. Girard, E. Tada, Fusion Eng. Des., **82**, 472 (2007).

[10] P. M. Komor, Nucl. Instrum. Methods. Phys. Res. B, **613**, 465 (2010).

[11] J. P. Carbajo, J. B. Parra, C. O. Ania, P. J. Merkling, S. Calero, ACS Appl. Mater. Interfaces, **11**, 18833 (2019).

[12] J. J. Urm, D. Park, J. U. Lee, M. H. Chang, J. M. Lee, Fusion Eng. Des., **172**, 112736 (2021).

[13] J. M. Bockris, D.B. Matthews, Electrochim. Acta, **11**, 143 (1966).

[14] M. Benedict, T. H. Pigford, H. W. Levi, McGraw-Hill Education, (1957).

[15] T. V. Vasyanina, I. A. Alekseev, S. D. Bondarenko, O. A. Fedorchenko, K. A. Konoplev, E. A. Arkhipov, V. V. Uborsky, Fusion Eng. Des., **83**, 1451 (2008).

[16] HA.Boniface, NV.Gnanapragasam, DK.Ryland, S.Suppiah, A.Perevezentsev, Fusion Scien. Tech., **71**, 241(2017)

[17] M. L. Hidalgo, S. Zhang, S. Hu, A. Esfandiar, I. V. Grigorieva, A. K. Geim, Nat

Commun, **8**, 15215 (2017).

[18] R. L. Borup, A. Kusoglu, K. C. Neyerlin, R. Mukundan, R. K. Ahluwalia, D. A. Cullen, K. L. More, A. Z. Weber, D. J. Myers, Curr Opin Electrochem, **21**, 192 (2020).

[19] S. T. Thompson, B. D. James, J. M. H. Kouadio, C. Houchins, D. A. DeSantis, R. Ahluwalia, A. R. Wilson, G. Kleen, J. Power Sources, **399**, 304 (2018).

[20] S. A. Grigoriev, V. I. Porembsky, V. N. Fateev, Int. J. Hydrog. Energy, **31**, 171 (2006).

[21] S. M. Saba, M. Mueller, M. Robinius, D. Stolten, Int. J. Hydrog. Energy, **43**, 1209 (2018).

[22] R. Tanii, R. Ogawa, H. Matsushima, M. Ueda, R. Dawson, Int. J. Hydrog. Energy **46**, 6745(2021)

[23] P. Li, L. Guo, R. Xiong, J. Luo, M. Wen, Y. Yao, Z. Zhang, J. Song, Y. Shi, T. Tang, C. J. Chemi. Engineering, **27**, 1837(2019)

[24] A.Pozio, S.Tosti, J. Hydrog. Energy, **44**, 7544(2019)

[25] M. Espinoza-andaluz, J. Santana, M. Andersson, Int. J. Hydrog. Energy, 45, 29763(2020)

[26] Y. Nonobe, IEEJ Trans, **12**, 5 (2017).

Chapter 2:

Effect of Water Vapor on Deuterium Separation by a Polymer Electrolyte Fuel Cell

2.1 Introduction

Development of a hydrogen-energy society is an ideal solution for decarbonization [1]. Water electrolysis and fuel cells play important roles in hydrogen production and utilization, respectively. Much attention has been paid to the electrode catalysts, cell structures, and system design of fuel cells [2–4]. As new hydrogen-energy technology, a fusion reactor is scheduled for completion in the 2030s [5]. In the fusion reactor, the hydrogen isotopes of deuterium (D) and deuterium (T) are used. Because T is a rare and radioactive material, it is necessary to circulate T in the fusion-reactor system as much as possible. The T concentration in the old fuel is upgraded to high purity, and the amount of T in the cooling water is recovered by an isotope-separation plant [6]. Therefore, separation/enrichment technology of hydrogen isotopes will be essential in the future.

Heavy water (D_2O) is obtained from natural water, in which the D concentration is very low (140 ppm). The Girdler-sulfide process [7, 8] and combined electrolysis catalytic exchange (CECE) method are used for production of D_2O [9, 10]. The former is the isotope-exchange reaction between water and hydrogen sulfide:

$$H_2O_l + HDS_g \leftrightarrow HDO_l + H_2S_g \tag{2.1}$$

where the subscripts l and g are the liquid and gas phase, respectively. The equilibrium constant of Eq. (2.1) depends on the temperature. Therefore, D is enriched by repeating the reaction at high and low temperatures.

CECE uses hydrogen gas produced by water electrolysis. The gas can exchange the isotopes with water by the following two steps:

$$HD_g + H_2O_v \leftrightarrow H_{2g} + HDO_v \quad (2.2)$$

$$HDO_v + H_2O_l \leftrightarrow H_2O_v + HDO_l \quad (2.3)$$

where the subscript v is the vapor phase. Equation (2.2) is the isotope-exchange reaction between the gas molecules on a catalyst. The reaction is called vapor-phase chemical exchange (VPCE). Equation (2.3) is a gas–liquid exchange reaction by evaporation and condensation. It occurs through the gas–liquid interface. For practical operation at low temperature, the combined reactions of Eqs. (2.2) and (2.3) are preferred as liquid-phase chemical exchange (LPCE). For example, suppose D enrichment from the gas phase to the liquid phase. When the HD_g concentration increases, the equilibrium of Eq. (2.2) shifts to the right so that the amounts of H_{2g} and HDO_v increase. The increase in the amount of HDO_v simultaneously shifts the equilibrium of Eq. (2.3) to the right. These successive equilibrium shifts efficiently produce HDO_l.

Kogel catalysts and Dixon gauze rings are used in LPCE [11]. The catalysts are platinum, on which the hydrogen-gas molecule dissociates into adsorbed H atoms. The exchange reaction of Eq. (2.2) occurs between an adsorbed atom and a water molecule. When the catalyst surface is wetted, the catalytic activity is lost owing to the barrier for gas adsorption. Therefore, it is important to prevent the catalyst from being wetted. To accomplish this, some hydrophobic substances are added to the platinum or platinum-alloy catalysts as supporting materials [12–16], and polytetrafluoroethylene (PTFE) is suitable in terms of fabrication and durability [17–19].

Polymer electrolyte fuel cells (PEFCs) also use PTFE in the catalytic layer (CL) and gas-diffusion layer (GDL) [20, 21]. The purpose of using PTFE is to prevent the flooding phenomenon, where the generated water is accumulated in the layers. Moreover,

the hydrophobic and hydrophilic materials are optimally blended so that many three-phase interfaces are created. This is an ideal environment for VPCE and LPCE. In the PEFC, the CL is formed by spraying the catalyst ink. Therefore, it is advantageous to produce a large surface area with a small amount of platinum.

D separation using PEFCs has been reported [22–28]. We found that D was enriched in the produced water when a PEFC was used with a mixture of H_2 and D_2 gases. The fuel-cell reactions consist of the following elementary kinetic steps: (1) oxidation of hydrogen gas at the anode ($L_2 \rightarrow 2L^+ + 2e^-$), (2) hydron diffusion in the membrane, and (3) reduction of hydron at the cathode ($O_2 + 2L^+ + 2e^- \rightarrow L_2O$), where L is the hydrogen isotopes. That is, it is suggested that the D reactions are kinetically faster than the H reactions.

Because our previous results included both VPCE and electrochemical factors, the kinetic considerations were inadequate. In this study, D separation by the isotope-exchange reaction and electrochemical reaction was individually measured at the same PEFC, and the D mass balance in the hydrogen gas and produced water was investigated.

2.2 Experimental

A gas mixture of H_2 and D_2 was supplied to the fuel cell. Both the hydrogen and oxygen gases were humidified by bubblers. The hydrogen gas from the anode was analyzed by a quadrupole mass spectrometer (QMS). First, water vapor was introduced to investigate VPCE. The effect of the electrochemical reactions during power generation was investigated.

2.2.1 Experimental Setup

A schematic diagram of the apparatus is shown in Fig. 2.1. A single PEFC (electrode area 5 cm × 5 cm) was tested. A carbon-supported platinum catalyst (0.3 mg cm^{-2}) and a PTFE-coated GDL (TGP-H-120, Toray, Japan) were used for both electrodes. Nafion (NRE 212, Dupont, USA) was used as the electrolyte membrane. Bubblers were installed on both sides to humidify the supplied gases. They were wrapped with band heaters (MBH 50-30, Misumi, Japan), and the temperature was adjusted to 40 °C by a heat controller (WCL-13A-SS/MM, Shinko Technos Co., Japan). Three-way valves were installed in both gas lines, and the bypass line (line A) was used for studying the dry gas.

All of the gases were supplied from cylinders. Pure H_2 and D_2 (99.9%) gases were used on the anode side, while N_2 and O_2 gases were used on the cathode side. The gas flow rate to the anode was 44 cc min^{-1} (H_2 40 cc min^{-1}, D_2 4 cc min^{-1}). The gas flow rates of the N_2 and O_2 gases were set to 40 cc min^{-1}. The flow rates were adjusted by a mass flow controller (MC 200 SCCM, Alicat Scientific, USA). The D concentration was set to 10 at%. A silicon belt heater (SBH 15, Sakaguchi E.H. Corp., Japan) was wrapped around both inlet pipe lines to prevent dew condensation after passing through the bubbler. Sheet heaters were placed on both sides of the cell, and the temperature was set to 65 °C.

The relative humidity was 28%.

The outlet gases were cooled to −20 °C by a cold trap (UT-1AS, ASONE Corp., Japan). The water vapor was condensed and collected as a liquid. The anode gas was analyzed by a QMS (HGM202, ULVAC Inc., Japan). Before starting the experiment, the valve (Figure 2.1-13) was switched to bypass the cell, and the anode inlet gas was fed through line B to the QMS.

The cell was electrically connected to an electronic load (PLZ164WA, Kikusui, Japan), and a constant current was generated. The temperature, dew point, and flow rate at the PEFC inlet/outlet were recorded by a digital logger (GL840, GRAPHTEC Corp., Japan).

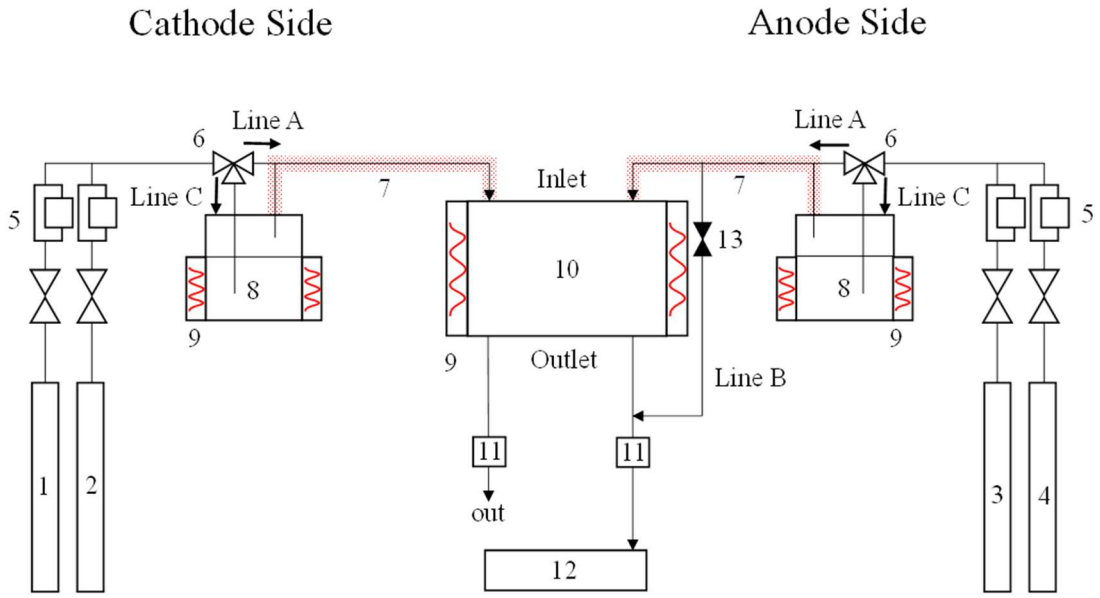

Figure 2.1 Schematic illustration of the experimental measurement setup. 1. O_2 gas cylinder. 2. N_2 gas cylinder. 3. D_2 gas cylinder. 4. H_2 gas cylinder. 5. Mass-flow controller. 6. Three-way valve. 7. Silicon belt heater. 8. Bubbler. 9. Band heater. 10.Fuel cell. 11. Cold trap. 12. Mass spectrometer. 13. Cell-bypass valve. 14. Electronic load. 15. Sample container.

2.2.2 Experimental Procedure

Measurements were successively performed by changing the humidity, O_2 gas, and power generation. The operation conditions are given in Table 2.1. Each step was continued until the QMS measurements reached a steady state. Hydrogen gas was introduced into the QMS, and the mass numbers of m = 2 (H_2), 3 (HD), and 4 (D_2) were measured.

The H/D ratio at the fuel-cell inlet was measured in step I. The gas mixture of H_2 and D_2 was directly flowed to the QMS through bypass lines A and B. The cathode gas was N_2 gas. Because O_2 gas crosses the membrane, the "direct reaction" ($L_2 + O_2 \rightarrow L_2O$) occurs on the anode catalyst [29]. We flowed N_2 gas to check the effect of this reaction on D separation. The feed gases for both electrodes were directly supplied from a cylinder without a bubbler. Power generation was not performed. In step II, the cell-bypass valve was closed and hydrogen gas was supplied to the cell. This procedure was performed to study the isotope-exchange reaction of the dry gas. In step III, the three-way valve was switched to the bubbler (from line A to line C in Fig. 2.1), and the feed gases were humidified. By including water vapor in the feed gases, VPCE can occur.

In step IV, the gas was switched from N_2 to O_2. It is presumed that the direct reaction occurs at the anode catalyst. Comparison with step III can clarify the effect of the direct reaction. In step V, the cell generated electricity of 1 A (J = 0.04 A cm^{-2}) to investigate D separation.

Table 2.1 The detail operation condition at each experimental step.

Step	Measurement Point	Gas at Cathode	Humidification	Generation Current (A)
I	Inlet	N_2	Dry	0
II	Outlet	N_2	Dry	0
III	Outlet	N_2	Wet	0
IV	Outlet	O_2	Wet	0
V	Outlet	O_2	Wet	1

2.2.3 Mass-Balance Analysis

The molar amounts of D in the gas and water phases were calculated. The results without and with power generation were obtained in steps III and V (Table 2.1), respectively. Under the present experimental conditions, the water produced by the cell was discharged as vapor. Therefore, the amount of water condensation collected in the cooling trap was weighed. The D concentration was determined by attenuated total reflection Fourier-transform infrared spectroscopy (FTIR-4200, JASCO International Corp., Japan). The concentration was calculated using a calibration curve previously measured with standard solutions. The D concentration in the gas from the anode was measured by the QMS. The gas volume was calculated by subtracting the gas volume consumed by power generation from the inlet flow volume. The measurement was performed for 10 h.

2.3 Results and Discussion

2.3.1 Separation Factor

The ion current change of the QMS is shown in Fig. 2.2. In step I, the current ratio of i_{H2} to i_{D2} was 10:1, which corresponded to the ratio of the gas flow rates. After the gas mixture passed through the cell (step II), the current values of i_{HD} and i_{D2} remarkably changed in opposite directions, while that of i_{H2} showed little variation. This is explained by the isotope-exchange reaction ($H_2 + D_2 \rightarrow 2HD$) on platinum. The exchange ratio was more than 98%. The high exchange efficiency means that both gases were well mixed in the GDL and the gas molecules contacted the catalyst well. When the gas was humidified (step III), the ion currents of i_{HD} and i_{D2} decreased. Introduction of humidified O_2 gas did not influence any of the ion currents (step IV), whereas power generation decreased i_{HD} and i_{D2} more than i_{H2}.

The [D]/[H] ratio was calculated from the stable ion currents in Fig. 2.2. The separation factor α was calculated by

$$\alpha = ([D]/[H])_{in}/([D]/[H])_{out} \quad (2.4)$$

where [L] is the atomic concentration in the hydrogen gas, and the subscripts in and out are the inlet and outlet gas, respectively. The ratio in each step refers to that of the inlet gas. The separation factor in each step is shown as a bar graph in Fig. 2.3. When dry gas was introduced into the cell (step II), D separation/condensation did not occur. When the gas was humidified, the D ratio in the outlet gas was diluted (step II). This is presumably due to the presence of water vapor inside the cell, which causes VPCE on the platinum catalyst. When humidified N_2 gas was switched to humidified O_2 gas (step IV), there was

no significant change in α. That is, the direct reaction, where O_2 gas permeates to the anode and reacts with hydrogen gas, did not contribute to D separation. Power generation increased α to 1.71 (step V). It should be noted that the value is the sum of VPCE and the electrochemical reaction. Supposing that α is the multiplication value in steps IV and V, the separation factor only by the electrochemical reaction was approximately 1.21.

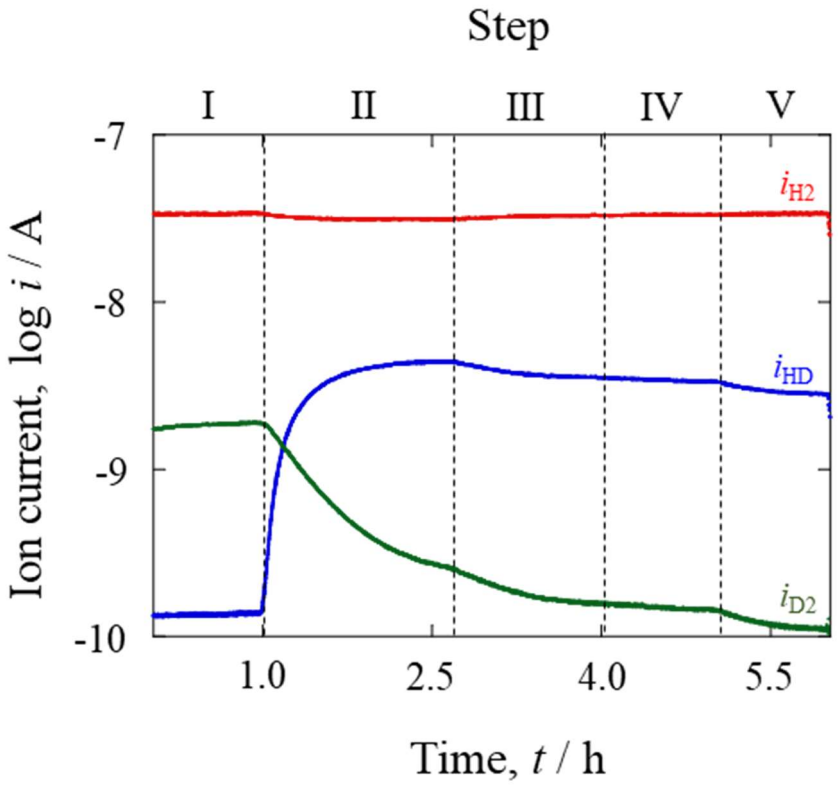

Figure 2.2 Transient behavior of the ion currents (iH_2 red, iHD blue, iD_2 green) of the hydrogen gas in each experimental step in Table 2.1. (For interpretation of the references to color/colour in this figure legend, the reader is referred to the Web version of this article.)

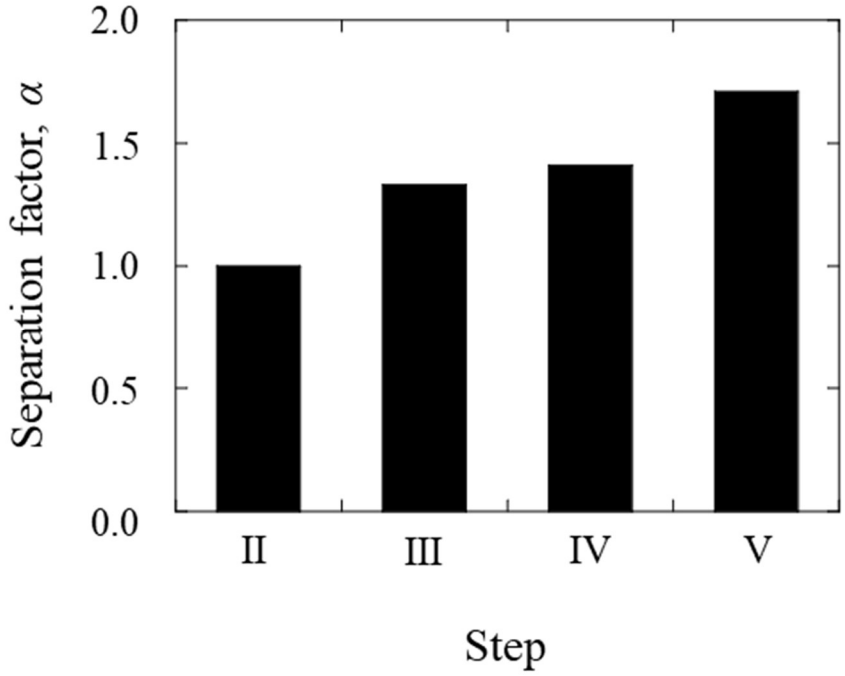

Figure 2.3 Bar chart of the separation factor, *a*, in each experimental step in Table 2.1.

2.3.2 Mass Balance

The present α value was smaller than previous reported values (α = 2–4) [22, 26]. The D concentration depends on the amount of the unreacted gas from the cell. That is, when the unreacted gas increases, α approaches 1. Therefore, we investigated how much D was directly transferred to water.

The weights of the water drainage and [D]/[H] ratios at the anode and cathode are given in Table 2. Without power generation, the water weights at the anode and cathode were the same, because water vapor was only supplied by the bubbler. When the cell reaction produces water, the amount of water approximately doubles. Interestingly, even though water was generated at the cathode, the water weight at the anode also increased.

Table 2.2 Results of water mass balance and [D]/[H] ratio at anode and cathode with or without generation.

	Without generation		With generation	
	Anode	Cathode	Anode	Cathode
A mount of water (g)	1.49	1.39	3.19	3.26
[H]/[D]	0.185	0.184	0.154	0.169

In a proton-exchange membrane, there are two types of water transport between the anode and cathode [30, 31]. The first type is diffusion by the difference in the water activities between the two electrodes. Water diffuses through the membrane to the anode because water is produced at the cathode during power generation. The second type is electroosmosis by hydron transfer, where hydrons generated at the anode move through the membrane to the cathode. In this type of diffusion, several water molecules are coordinated to the hydron and are dragged together with the hydron. That is, the two types of water transport, diffusion and electro-osmosis, are opposite. The present result, where the same amounts of water were discharged from both electrodes, suggested predominance of diffusion. Because the power current was low, few hydrons transferred, and thus electro-osmosis drag could be negligible.

The [D]/[H] ratio in the drainage water was approximately 1.5–1.8 times larger than that of the inlet gas ([D]/[H] = 0.10). The D concentration in water is enriched by VPCE and the cell reaction. Without power generation, the ratios at the cathode and anode were the same, even though VPCE only occurs at the anode. The D activity at the anode is higher than at the cathode. Therefore, the activity difference may induce preferential D diffusion to the cathode, but the total water activities are the same at both electrodes. When power was generated, the [D]/[H] ratio was higher at the cathode than at the anode. This suggests the D was concentrated in the water by the electrochemical reduction reaction at the cathode ($O_2 + 2L^+ + 2e^- \rightarrow L_2O$). In addition, the gradient of the water content between both electrodes might contribute to the D concentration difference.

The breakdown of the D amounts in the gas and water phases is shown in Fig. 2.4. The D molar mass (107 mmol) in the inlet gas was almost equal to the sum of those

in the outlet gas and water, regardless of power generation. D did not remain or was adsorbed in the cell. With no power generation, a quarter of the D molar mass in the gas was converted to vapor, while approximately 45% of the D molar mass was transferred to water during power generation. The cell reaction recovered more D than VPCE. As previously mentioned, the separation ability of the cell reaction seems to be small, because the α value is calculated only from the gas component. Actually, in terms of mass balance, D was efficiently converted to water by both VPCE and cell reactions.

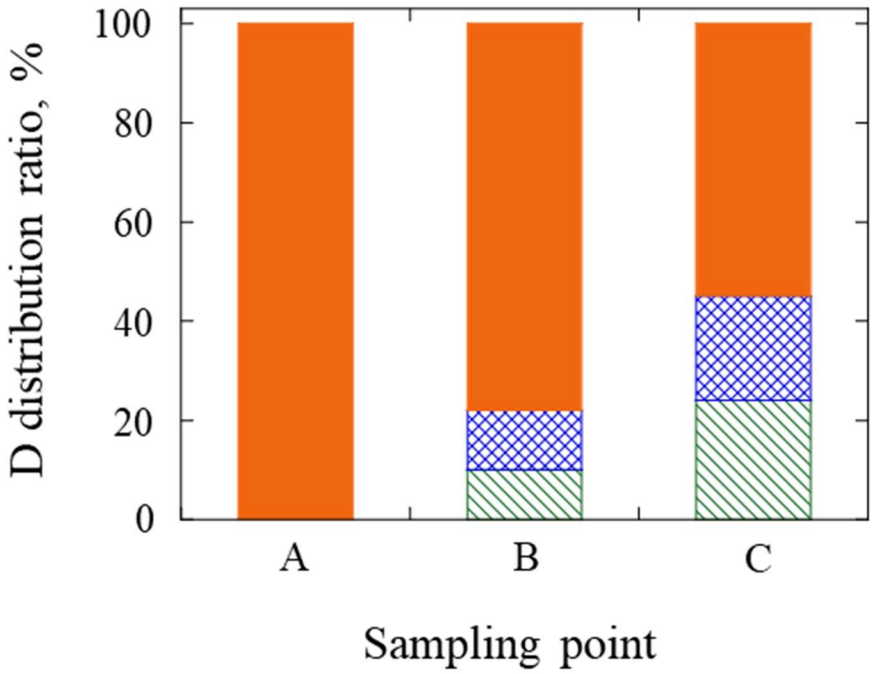

Figure 2.4 Bar chart of the D distribution breakdown ratio for each sampling point and power condition (A, inlet; B, outlet without power generation; C, outlet with power generation; filled orange area, gas in the anode; blue lattice area, water in the anode; green downward diagonal area, water in the cathode). (For interpretation of the references to color/color in this figure legend, the reader is referred to the Web version of this article.)

2.3.3 Equilibrium Constant of VPCE

We will discuss VPCE when no power is generated. Rolston et al. [32] reported the experimental relationship between the equilibrium constant of Eq. (2.2) (K_1) and the temperature (T):

$$\ln K_1 = -0.02735 + 449.2/T + 2380/T^2 \tag{2.5}$$

In the present experiment at 65 °C, K_1 = 2.93. K_2 is determined by the gas pressure as follows:

$$K_2 = P_{HDO}/P_{H2O} \times P_{H2}/P_{HD} \tag{2.6}$$

where P_x is the partial gas pressure of component x. Suppose that the P_{HDO}/P_{H2O} ratio is the molar ratio of HDO (25.3 mmol) to H_2O (56.1 mmol) at the anode outlet, then P_{HDO}/P_{H2O} = 0.45. When the P_{H2}/P_{HD} ratio is calculated from the ion current of the QMS, P_{H2}/P_{HD} = 7.18. Substituting the ratio values into Eq. (2.6) gives K_2 = 3.24. This value agrees with K_1 of Eq. (2.5). This supports that the vapor and gas were well mixed in the GDL and the reaction reached equilibrium in the compact fuel cell. The ideal results also mean no droplet formation on the catalyst.

2.4 Conclusions

D separation experiments have been performed using a PEFC with a gas mixture of H_2 and D_2 at room temperature. When the PEFC did not generate power and the gases were humidified, D was enriched in the water vapor by VPCE. The direct reactions by O_2 crossover did not contribute to D separation. When the PEFC generated power, D was more efficiently separated. The separation factor was approximately 1.7, while it was approximately 1.3 for only VPCE.

The D mass balance results showed no D retention in the PEFC. From the D distribution breakdown, approximately 20% of D in the inlet gas was transferred to the water vapor by VPCE. Power generation produced enriched D water and increased the transport ratio to approximately 50% D. The difference of the D concentrations between the cathode and anode was not significant.

The D mass balance without power generation made it possible to calculate the equilibrium constant of VPCE. The equilibrium constant was almost the same as the reported value. This supported that the PEFC could separate D without any wetting problems. The present results demonstrate the synergistic effect of VPCE and the electrochemical reaction on D separation.

References

[1] M. Yue, H. Lambert, E. Pahon, R. Roche, S. Jemei, D. Hissel, *Renew. Sustain. Energy Rev.*, **146**, 111180 (2021).

[2] J. Cai, R. Javed, D. Ye , H. Zhao, J. Zhang, *J. Mater. Chem. A*, **43**, 22467 (2020).

[3] A. H. Gomez, V. Ramirez, D. Guilbert, *Int. J. Hydrog. Energy*, **45**, 14625 (2020).

[4] A. Biyikoglu, *Int. J. Hydrog. Energy*, **30**, 1181 (2005).

[5] B.G. Hong, *Int. J. Hydrog. Energy*, **42**, 4 (2018).

[6] M.H. Chang, S.H. Yun, H.G. Kang, S. Cho, K.M. Song, D. Kim, H. Chung, P. Camp, W. Shu, S. Willms, M. Glugla, *Fusion Eng. Des.*, **89**, 1557 (2014).

[7] J.L. Aprea, *Int. J. Hydrog. Energy*, **27**, 741 (2002).

[8] B.M. Andreev, *Sep. Sci. Technol.*, **36**, 1949 (2001).

[9] Y. Xu, F. Xin, Y. Jiang, X. Yin, *ACS Appl. Mater. Interfaces*, **13**, 31660 (2021).

[10] T. Sugiyama, Y. Asakura, T. Uda, T. Shiozaki, Y. Enokida, I. Yamamoto, *Fusion Eng. Des.*, **81**, 833(2005).

[11] T. Sugiyama, A. Ushida, I. Yamamoto, *Fusion Eng. Des.*, **83**, 1447(2008).

[12] L. Ye, D. Luo , W. Yang, W. Guo, Q. Xu, L. Luo, *Int. J. Hydrog. Energy*, **39**, 13793 (2014).

[13] L. Ye, D. Luo, W. Yang, W. Guo, Q. Xu, C. Jiang, *Int. J. Hydrog. Energy*, **38**, 13596 (2013).

[14] S. Hu, J. Hou, L. Xiong, K. Weng , T. Yang , Y. Luo, *Sep. Purif. Technol.*, **77**, 214 (2011).

[15] S. Hu, L. Xiong, J. Hou, K. Weng, Y. Luo, T. Yang, *Int. J. Hydrog. Energy*, **35**, 10118 (2010).

[16] K. Kawakami, Y. Takao, K. Kusunoki, *Can. J. Chem. Eng.*, **64**, 432 (1986).

[17] F. Huang, *Int. J. Hydrog. Energy*, **43**, 1718 (2018).

[18] F. Huang, C. Meng, *Int. J. Hydrog. Energy*, **35**, 6108 (2010).

[19] N. M. Gupta, A. D. Belapurkar, K. V. S. Ramarao, R.M. Iyer, *Applied Catalysis*, **43**, 15 (1988).

[20] G. G. Park, Y. J. Sohn, T. H. Yang, Y. G. Yoon, W. Y. Lee, C. S. Kim, *J. Power Sources*, **131**, 182 (2004).

[21] G. Lin, T. V. Nguyen, *J. Electrochem. Soc.*, 152, A1942 (2005).

[22] A. Pozio, S. Tosti, *Int. J. Hydrog. Energy*, **44**, 7544 (2019).

[23] R. Tanii, R. Ogawa, H. Matsushima, M. Ueda, *Int. J. Hydrog. Energy*, **44**, 1851 (2019).

[24] R. Ogawa, R. Tanii, R. Dawson, H. Matsushima, M. Ueda, *Energy*, **149**, 98 (2018).

[25] R. Ogawa , H. Matsushima , M. Ueda, *Electrochem. Commun.*, **70**, 5 (2016).

[26] S. Shibuya, H. Matsushima, M. Ueda, *J. Electrochem. Soc.*, **163**, F704 (2016).

[27] S. Yanase, T. Oi, *J. Nucl. Sci. Tchnol.*, **50**, 808 (2013).

[28] M. P. M. Kaninski, V. M. Nikolic, A. D. Maksic, G. S. Tasic, S. S. Miljanic, *Electrochem. Commun.*, **10**, 1463 (2008).

[29] M. Seddiq, H. Khaleghi, M. Mirzaei, *J. Power Sources*, **161**, 371 (2006).

[30] E. J. F. Dickinson, G. Smith, *Membranes*, **10**, 11 (2020).

[31] K. Harada, R. Tanii, H. Matsushima, M. Ueda, K. Sato, T. Haneda, *Int. J. Hydrog. Energy*, **45**, 31389 (2020).

[32] J. H. Rolston, J. D. hartog, J. P. Butler, *J. Phys. Chem.*, **80**, 1064 (1976).

Chapter 3:

Application of Membrane Electrode Assembly for Water Hydrogen Isotope Exchange

3.1 Introduction

Hydrogen energy is one solution for a decarbonized society. Hydrogen has three isotopes: protium (H), deuterium (D), and tritium (T). D has been used as a moderator in nuclear power plants. It is applied to hydrogen termination of Si to increase the durability of semiconductors [1]. T and D will be essential materials for fusion reactors, while it is important to manage the T concentration in the cooling water [2, 3]. The isotopes separation technology will be more important in the near future.

There are various hydrogen isotope separation methods, including cryogenic distillation [4], chemical exchange [5-8], and water electrolysis [9-11]. New separation ones, using zeolite [12] and graphene [13], have also been discovered. The water-hydrogen exchange process, which is the simplest in the chemical exchange reactions, will be employed in ITER. It is used with water electrolysis as CECE (combined electrolysis and catalytic exchange).

In CECE, water containing D and T is electrolyzed initially. The hydrogen gas of HT and HD is reacted with H_2O solution flowing from top of the catalytic tower. T and D is transferred to water solution. For example, when H and D are considered, the reactions are expressed by following three-steps;

$$H_2(g) + D_2(g) \leftrightarrow 2HD(g) \tag{3.1}$$

$$HD(g) + H_2O(v) \leftrightarrow H_2(g) + HDO(v) \tag{3.2}$$

$$HDO(v) + H_2O(l) \leftrightarrow H_2O(v) + HDO(l) \tag{3.3}$$

where g is gas, v is vapor, and l is liquid.

On one hand, platinum is usually used in the catalytic reaction, Eq. (3.2).

Hydrogen gas molecules dissociate into adsorbed atoms on the surface. The isotope exchange occurs between the adsorbed atoms and water vapor. Therefore, once the catalyst is wetted, the gas cannot reach the surface so that the activity is lost. For this reason, a hydrophobic treatment on the catalyst is performed because the catalyst is in well contact with the gas phase. Some hydrophobic materials are proposed [14-16], and particularly polytetrafluoroethylene (PTFE) is suitable in terms of fabrication and durability [17]. Equation (3.3) is occurred through the gas-liquid interface, on the other hand. Dispersion of liquids is effective in improving the reaction. Therefore, hydrophilic fillers (Dixon gauze rings) are commonly used.

The reaction columns contain a mixture of substances with different wettability, therefore, making it necessary to consider complex mass transfer of liquid and gas [18-21]. In addition, small hydrophobic catalysts, which do not allow water easily passing through, cause flooding in the columns. This requires a large size of equipment where Kogel catalysts with much platinum is used.

As an ideal structure to solve above problems, we have considered the membrane electrolyte assembly (MEA) used in polymer electrolyte fuel cells (PEFCs) [22-24]. MEA is consisted of the porous catalyst layer (CL) and gas diffusion layer (GDL) [25]. The membrane utilizes PTFE to prevent flooding by water production during the power generation. In MEA, many three-phase interfaces are formed by optimal blending of hydrophobic and hydrophilic substances [26]. This is suitable for the water-hydrogen exchange reactions. Moreover, the CL is formed by spraying catalytic ink, which is in favor of creating a large surface area with a small amount of platinum.

We reported that the mixture of H_2 and D_2 gas was used in PEFCs and enriched in the production water during power generation. Interestingly, the previous results

suggested that D was concentrated in the vapor only when the mixture gas passes through PEFC [22]. However, due to the operational limitation of our PEFC where water vapor was not controlled, it was impossible to check the exchange reactions carefully. Here, by controlling the amount of relative humidity in PEFC, we intentionally allowed condensation in PEFC and investigated the exchange reactions. In order to quantitatively evaluate the mass balance of D in the gas and vapor, the mass transportation in the PEFC was discussed.

3.2 Experimental

The experimental setup, including gas supply, has been described in detail in the previous paper [22]. Here, several essential parts are explained.

PEFC was standard JARI cell (FC Development Corp., Japan) with a 25 cm^2 electrode area. It was consisted of two stainless endplates, a carbon separator, and an MEA (Fig. 3.1). The separator had a groove (1×1mm) in the center where the feed gas can flow. The channel was a single serpentine. When the MEA was enlarged, the separator contacted the GDL made by porous carbon fiber. The PTFE coated GDL (TGP-H-120, Toray, Japan) was used. On the opposite GDL surface, a porous CL was formed. The CL was prepared by spraying the ink with dispersed platinum-loaded carbon. The electrolyte membrane was a cation exchange one (NRE 212, Dupont, USA).

The hydrogen and nitrogen gas were supplied to the anode and cathode, respectively. The feed rates were controlled by mass flow controllers (MC 200 SCCM, Alicat Scientific, USA). Hydrogen gas was H_2 (40 cc min^{-1}) and D_2 (4 cc min^{-1}), while an inlet nitrogen gas flow was 40 cc min^{-1}(25 °C, 0.1 MPa). The settings were selected as the same flow rate as in the previous paper [22]. This setting value was set as about twice the stoichiometric value when the fuel cell generates electricity at 0.1 A cm^{-2}. Water vapor was supplied to the feed gas by a bubbler. The bubbler was equipped with a heater to control the temperature in the range of 25 °C to 65 °C. The gas lines were heated by ribbon heaters to prevent vapor condensation. Hydrogen gas, vapor, and dew water were discharged from the cell. The gas-liquid flows were separated in a gas-liquid separator. While the liquid was stored in a reservoir directly, the vapor was collected by passing the gas through a condenser (-20 °C). The D concentration in water was measured by ATR-FTIR (FTIR-4200, JASCO International Corp., Japan). The dried gas was introduced into

the quadrupole mass spectroscopy (HGM202, ULVAC Inc., Japan), and mass numbers of 2 (H_2), 3 (HD), and 4 (D_2) were measured.

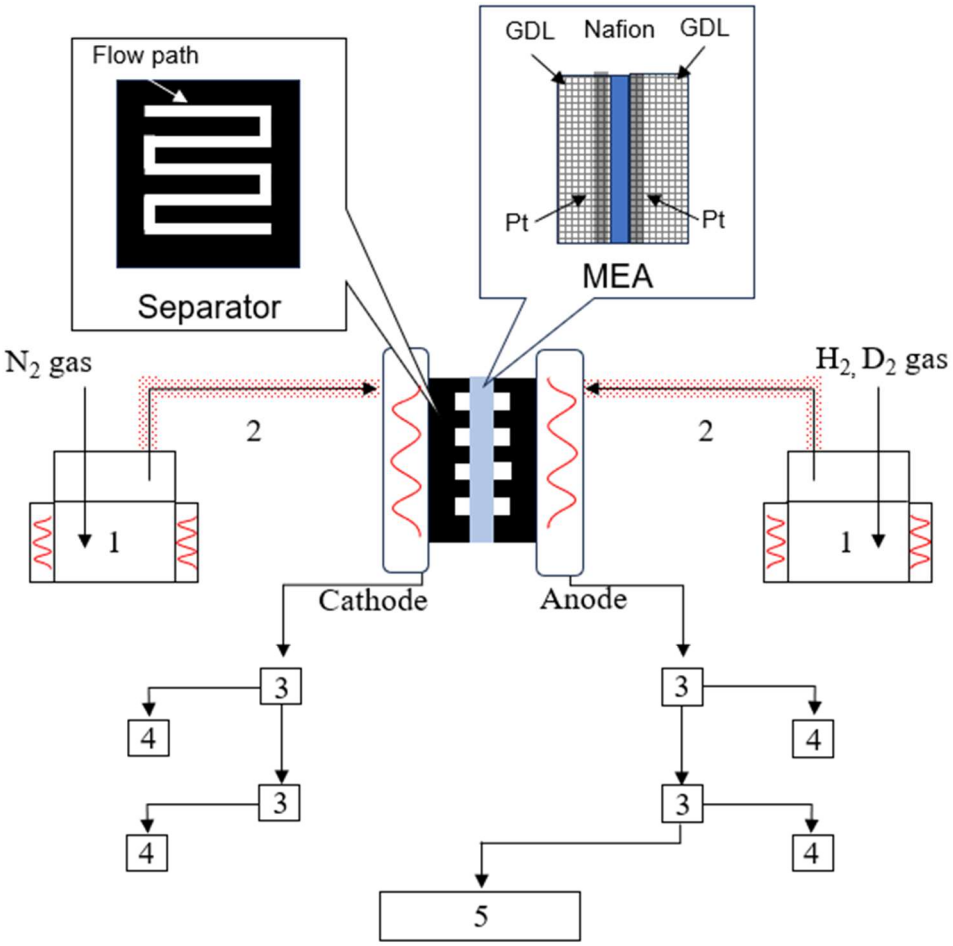

Figure 3.1 Schematic illustration of the experimental measurement setup;
1: Bubbler, 2: Ribbon heater, 3: Gas-liquid separator, 4: Cold trap and liquid container, 5: Quadrupole mass spectroscopy.

3.3 Results and discussion

The bubbler and cell temperatures were adjusted to control the water dew rate. Three different cell temperatures were selected depending on the bubbler one (40, 50, and 60 °C). When the cell temperature is lower than the dew point of the supply gas (bubbler temperature), T_d, water condensation occurs.

Table 3.1 summarizes the experimental conditions. The temperature of the supplied gas was from 40°C to 60°C, which was the normal temperature range of the fuel cell. The cell temperature was 5°C higher than the dew point of the supplied gas in order to prevent condensation water inside the fuel cell (conditions 3, 6, and 9). For each dew point, the cell temperature was varied to three levels. One is from 5 to 10°C lower than the supply gas temperature (conditions 2, 5, and 8) and the other is from 25 to 30°C lower (conditions 1, 4, and 7).

From T_d (°C), the saturated water vapor pressure, P_w (kPa), is calculated and water quantity in vapor, Q_w (g m^{-3}), is derived from the gas state equation as follows,

$$P_W = 0.61078 \times 10^{\frac{7.5 \times T_d}{(T_d+237.3)}} \tag{3.4}$$

$$Q_W = 217 \times \frac{P_W}{(T_d+273.1)}. \tag{3.5}$$

The flow rate of water vapor, V_f (mmol min^{-1}), is obtained from the volume rate of the feed gas, F (m^3 min^{-1}),

$$V_f = F \times Q_w. \tag{3.6}$$

In the cell, the flow rate of dew condensation, D_{cell} (mmol min^{-1}), is estimated by subtracting the vapor content in the cell, V_{cell} (mmol min^{-1}), from V_f,

$$D_{cell} = V_f - V_{cell} \tag{3.7}$$

where V_{cell} is obtained from Eqs. (3.4-3.6) using the cell temperature, T_{cell}(℃).

The separation factor, α, is determined to quantitatively examine the change in D concentration in hydrogen gas. Here, the concentration ratios of H and D is defined as following [22],

$$\alpha = ([H]/[D])_{out}/([H]/[D])_{in} \tag{3.8}$$

in where subscript of out and in mean feed and discharge from the cell, respectively.

To investigate the effect of vapor condensation, α is plotted against the ratio of condensation water flow rate to vapor one, $R_{H2O} = D_{cell}/V_f$, in Fig. 3.2. The dotted lines in the Fig.3.2 are connected between plots. The D concentration in the gas decreased through the cell since α was larger than 1. As previously reported [22-24], it was explained by water-hydrogen exchange reaction where D was transported to vapor (Eq. 2), or dew condensation water (Eq. 3.3).

Table 3.1 Experimental setpoints and conditions in each test conditions

Test No.	Setpoint		Condition			
	T_d (°C)	T_{cell} (°C)	Q_w (g/m^3)	V_f (mmol/min)	D_{cell} (mmol/min)	R_{H2O}
1	40	25	51.1	0.056	0.066	1.21
2	40	35	51.1	0.096	0.028	0.29
3	40	45	51.1	0.159	0.000	0.00
4	50	25	82.8	0.056	0.146	2.59
5	50	40	82.8	0.125	0.078	0.62
6	50	55	82.8	0.254	0.000	0.00
7	60	30	129.8	0.074	0.243	3.27
8	60	50	129.8	0.202	0.115	0.57
9	60	65	129.8	0.317	0.000	0.00

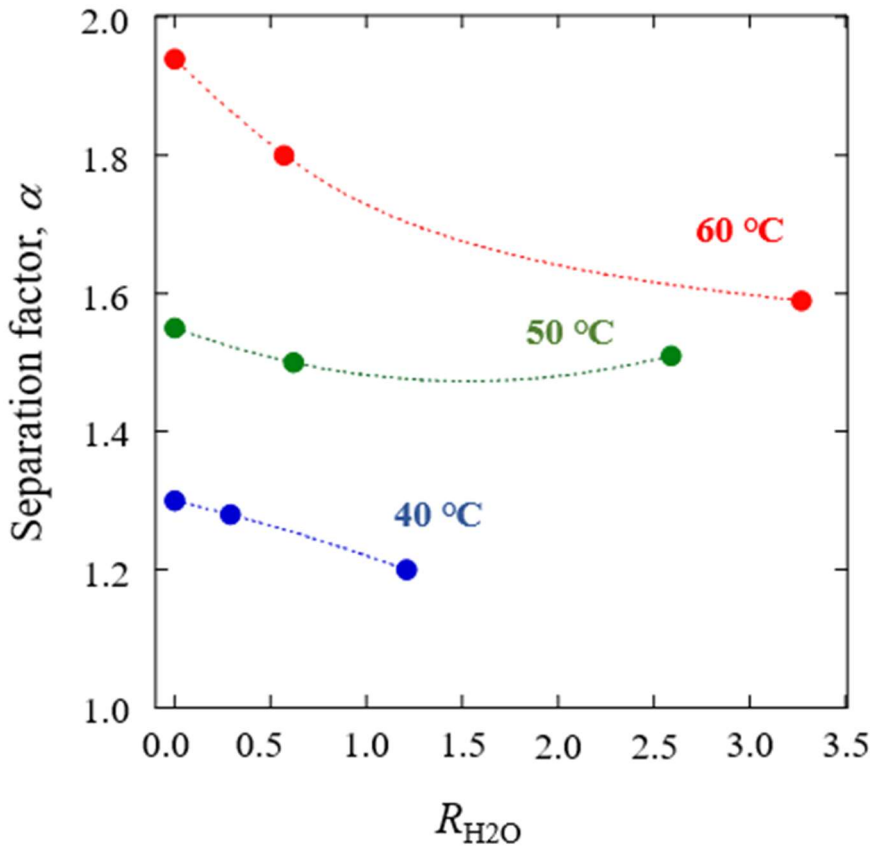

Figure 3.2 The effect of vapor condensation ratio, R_{H2O}, on α at various T_d (blue symbols: 40 °C, green one: 50 °C, red one: 60 °C).

The bubbler temperature influenced α. Figure 3.2 demonstrated that the high temperature improved the separation. It might be attributed to the equilibrium shift in Eq. (3.2). When T_d is high, the amount of water vapor increases. It is Q_w = 51 g m^{-3} at 40 °C, Q_w = 83 g m^{-3} at 50 °C, and Q_w = 130 g m^{-3} at 60 °C. That is, the equilibrium in Eq. (3.2) moves to the right direction at high temperature, resulting in more HDO(V) production. Interestingly, the separation performance was barely dependent on R_{H2O}. In higher vapor content (red plots), α decreased with increasing RH2O.

We calculated the amount of conversion how much D was shifted to water vapor or dew. In each elemental step, the amount of D conversion is considered as *X* at Eq. (3.1), *Y* at Eq. (3.2), and *Z* at Eq. (3.3). When the equilibrium constant at Eq. (3.1) is denoted as K_1, Eq. (3.1) is expressed using the amount of conversion,

$$K_1 = \frac{[HD(g)]^2}{[H_2(g)][D_2(g)]} = \frac{(2X\text{-}Y)^2}{(M_A\text{-}X+Y)(M_B\text{-}X)} \tag{3.9}$$

where M_A is the initial molar quantity of H_2 and M_B is that of D_2.

Using the equilibrium constants K_2 and K_3 in Eq. (3.2) and (3.3), the equations are defined as follows,

$$K_2 = \frac{[HD(g)][H_2O(v)]}{[H_2(g)][HDO(v)]} = \frac{(2X\text{-}Y)(M_C\text{-}Y+Z)}{(M_A\text{-}X+Y)(Y\text{-}Z)} \tag{3.10}$$

$$K_3 = \frac{[HDO(v)][H_2O(l)]}{[H_2O(v)][HDO(l)]} = \frac{(Y\text{-}Z)(M_D\text{-}Z)}{(M_C\text{-}Y+Z)\times Z} \tag{3.11}$$

where M_C is the initial molar quantity of vapor, M_D is that of liquid. The equilibrium constants are obtained from previous studies by Rolson et al. [27].

The value of *X*, *Y*, and *Z* are calculated from the series of Eqs. (3.9-3.11). To investigate the effect of dew condensation, Fig. 3.3 plotted them against R_{H2O}. The filled plots show the experimental value, and the unfilled plots show the calculated value. The dotted and solid line is an approximate curve predicted from experimental and calculated value, respectively.

The feed D_2 gas (53 mmol s^{-1}) was converted to HD very well. The result was supported by *X*. That was, the exchange reaction of Eq. (3.1) was independent of water vapor and dew condensation water (Fig. 3.3a).

The calculation (filled plots) show that *Y* were varied much (Fig. 3.3b). It was estimated that about 30% of HD gas was converted to HDO at 40°C (blue filled plots), 50% at 50°C (green ones), and 70% at 60°C (red ones). This is attributed to the feed vapor significantly depended on the bubbler temperatures (Q_w in Table 1). The experimental results (unfilled plots) at each temperature were less than the calculation. The difference decreased with increasing $R_{H2O} > 2.5$.

Fig. 3.3c shows the D transportation from HDO(v) to HDO(l). The calculated values (filled plots) increased as R_{H2O} increased. Much water was produced as the dew water, when the difference between T_d and T_{cell} was large. This means the equilibrium of Eq. (3.3). shifts in the right direction under the consideration of each concentration, although the phase change reaction between vapor and liquid phase might affect. For instance, more than 70% of HDO(v) was converted to HDO(l) at the conditions of No. 4 and 7 in Table 1. However, the experimental results (unfilled plots) were significantly smaller than the calculated ones. Despite the increase in R_{H2O}, HDO(l) did not increase much. The conversion to HDO(l) was only a few percent at T_d = 60 °C.

One possible reason for the small α in Fig. 3.2 is that there was not enough vapor

in the cell. Fig. 3.3b supported that the vapor in the cell was smaller than calculated one. The dew condensation consumed the vapor, resulting in decreasing V_f. On the other hand, when R_{H2O} increased, that of HDO(v) to HDO(l) would also increase. But this was not confirmed in Fig. 3.3c. Therefore, we investigated the HDO condensation ratio, R_{HDO} = HDO(l)/HDO(v). Figure 3.4 shows the comparison between the experimental value, R_{HDO_E}, and calculation one, R_{HDO_C}. The dotted lines in Fig. 3.4 are connected between plots. Clearly R_{HDO_E} was smaller than R_{HDO_C}. As the vapor pressure increased with T_d, the vapor-to-liquid conversion of HDO was very poor.

One of reasons is that the exchange reaction at Eq. (3.2) was less than half of the calculation, as shown in Fig. 3.3b. The GDL and Pt catalyst layers are composed of porous media in Fig. 3.1. Thus, when condensation occurs in pores, mass transportation of hydrogen gas and water vapor to the catalyst would be inhibited. In particularly, dew condensation water in the catalyst layer may cover the finer catalyst surfaces and the catalyst becomes deactivated. Water condensation may also occur in grooves in the separator. This does not contribute to the formation of a gas-liquid interface, and the exchange reaction in Eq. (3.3) hardly occurs.

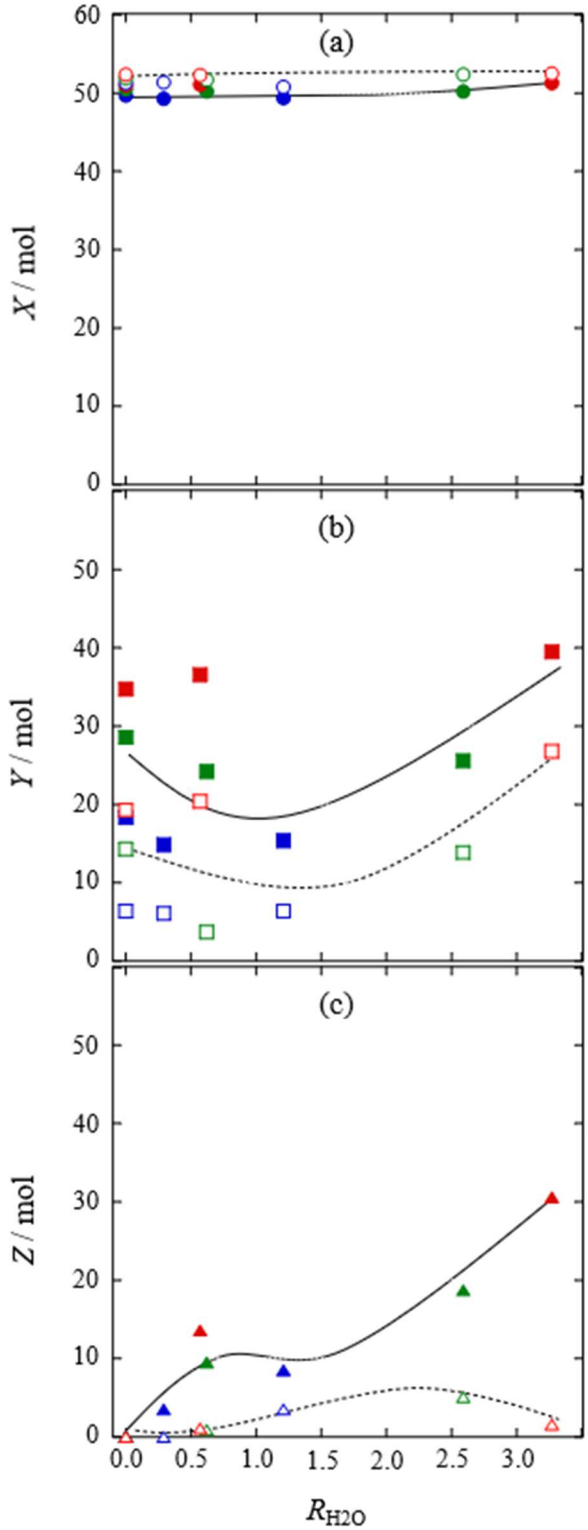

Figure 3.3 Dependency of conversion quantity on R_{H2O} at various T_d (blue symbols: 40 °C, green one: 50 °C, red one: 60 °C, filled ones: calculation, unfilled one: experiment). Figure (a) is X from D_2(g) to HD(g), Figure (b) is Y from HD(g) to HDO(v), and Figure (c) is Z from HDO(v) to HDO(l).

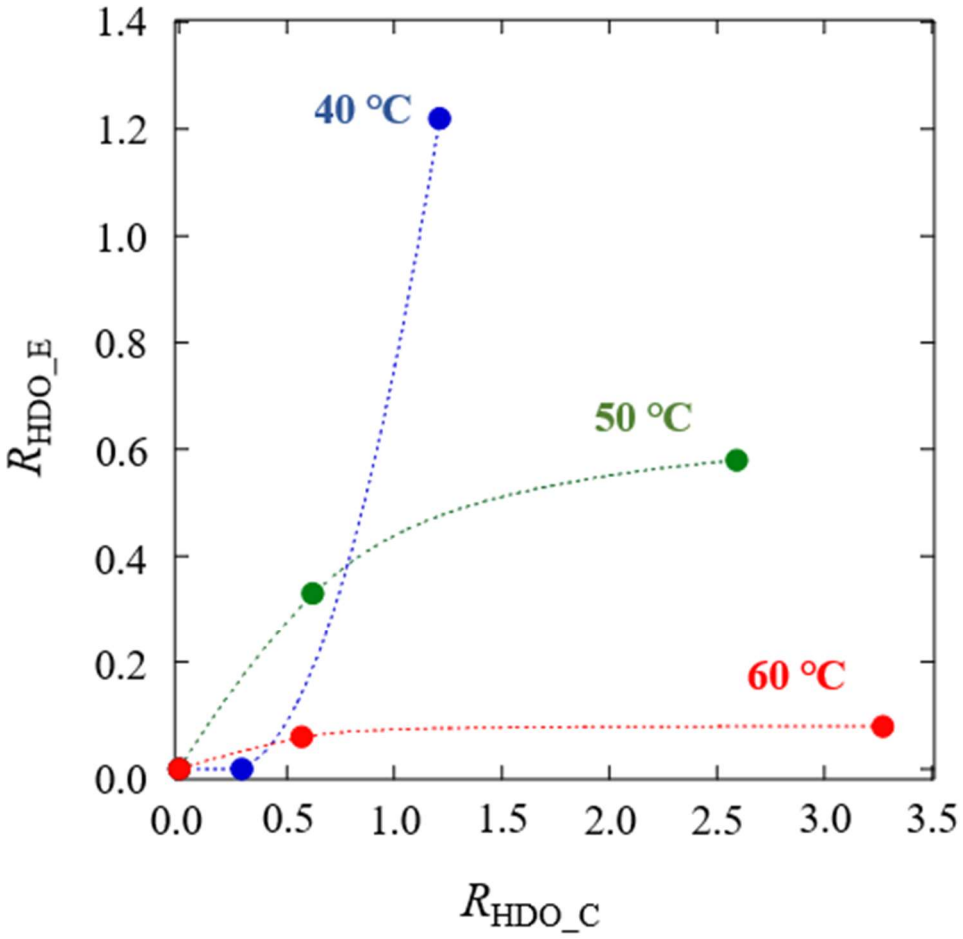

Figure 3.4 Comparison between the experimental HDO(l) dew ratio, R_{HDO_E}, and calculation one, R_{HDO_C}, at various T_d (blue symbols: 40 °C, green one: 50 °C, red one: 60 °C).

3.4 Conclusions

Water hydrogen isotope exchange was conducted using the mixture gas of H2 and D2. We applied MEA structure in PEFC for the separation directly. The vapor pressure in the mixture gas was controlled and the dew water was produced in the cell. The D conversion rate from gas thorough vapor to dew water was measured and calculated. The followings were concluded.

1. The value of α increased from 1.2 at 40 ℃ to 1.9 at 60 ℃. The separation was slightly suppressed by the dew water production, R_{H2O}.
2. According to the amount of conversion, X, Y, and Z, the supplied gases converted fully to HD gas, while D was transferred to neither vapor nor dew water as estimated from equilibrium constant. The present results showed that about 20% D of the feed gas was recovered as HDO water.
3. The large gap between R_{HDO_E} and R_{HDO_C} suggested that the condensation in the cell reduced the quantity of water vapor and that the dew inhibited the separation reaction because of wetting the catalyst surface.

References

[1] Gupta P., Colvin V.L., George S.M., *Phys. Rev. B*, **37**, 8234 (1988).

[2] Bellanger G., *Fusion Eng. Des.*, **84**, 2197 (2009).

[3] Iwai Y., Yamanishi T., Nakamura H., Isobe K., Nishi M., Willms R.S., *J. Nucl. Sci. Technol.*, **39**, 661 (2002).

[4] Bhattacharyya R., Bhanja K., Mohan S., *Int. J. Hydrog. Energy*, **41**, 5003 (2016).

[5] Kim H., Singh B.K., Um W., *J. Ind. Eng. Chem.*, **121**, 264 (2023).

[6] Xu Y.S., Xin F., Jiang Y., Yin X.H., *ACS Appl. Mater. Interfaces*, **13**, 31660 (2021).

[7] Sugiyama T., Asakura Y., Uda I., Shiozaki T., Enokida Y. Yamamoto I., *Fusion Eng. Des.*, **81**, 833 (2005).

[8] Aprea J.L., *Int. J. Hydrog. Energy*, **27**, 741 (2002).

[9] Xu J.S., Li R., Yan X.Y., Zhao Q.K., Zeng R.G., Ba J.W., Pan Q.F., Xiang X., Meng D.Q., *Nano Research*, **15**, 3952 (2022).

[10] Sato H., Matsushima H., Ueda M., Ito H., *Int. J. Hydrog. Energy*, **46**, 33689 (2021).

[11] Harada K., Tanii R., Matsushima H., Ueda M., Sato K., Haneda T., *Int. J. Hydrog. Energy*, **45**, 31389 (2020).

[12] Perez-Carbajo J., Parra J.B., Ania C.O., Merkling P.J., Calero S., *ACS Appl. Mater. Interfaces*, **11**, 18833 (2019)

[13] Yasuda S., Matsushima H., Harada K., Tanii R., Terasawa T.O., Yano M., Asaoka H., Gueriba J.S., Dino W.A., Fukutani K., *ACS Nano*, **16**, 14362 (2022).

[14] Li C., Chen H.L., Fan Y., Fu K., Liu C.L., Ren X.Y., Yang H.J., Lin S.D., *Int. J. Hydrog. Energy*, **48**, 3520 (2023).

[15] Ye L.S., Luo D.L., Yang W., Guo W.S., Xu Q.Y., Luo L.Z., *Int. J. Hydrog. Energy*,

39, 13793 (2014).

[16] Hu S., Hou J.W., Xiong L.P., Weng K.P., Yang T.Z., Luo Y.M., *Separ. Purif. Technol.*, **77**, 214, (2011).

[17] Huang F., *Int. J. Hydrog. Energy*, **43**, 171 (2018).

[18] Bukin A.N., Moseeva V.S., Ovcharov A.V., Marunich S.A., Pak Y.S., Rozenkevich M.B., *Fusion Eng. Des.*, **171**, 112595 (2021).

[19] Aldehani M., Alzahrani F., Saoir M.N.A., Fernandes D.L.A., Assabumrungrat S., Aiouache F., *Chem. Eng. Process*, **108**, 58 (2016).

[20] Ye L., Luo D., Tang T., Yang W., Zhao P., *Int. J. Hydrog. Energy*, **39**, 6604 (2014).

[21] Kumar R., Mohan S., Mahajani S.M., *Ind. Eng. Chem. Res.*, **52**, 10935 (2013).

[22] Furusawa K., Nago T., Ueda M., Matsushima H., *Int. J. Hydrog. Energy*, **47**, 36248 (2022).

[23] Ogawa R., Tanii R., Dawson R., Matsushima H., Ueda M., *Energy*, **149**, 98 (2018).

[24] Shibuya S., Matsushima H., Ueda M., *J. Electrochem. Soc.*, **163**, F704 (2016).

[25] Sinha P.K., Mukherjee P.P., Wang C.Y., *J. Mater. Chem.*, **17**, 3089 (2007).

[26] Liu Q.S., Lan F.C., Chen J.Q., Zeng C.J., Wang J.F., *J. Power Sources*, **517**, 230723 (2022).

[27] Rolston J. H., Denhartog J., Butler J.P., *J. Phys. Chem. A*, **80**, 1064 (1976).

Chapter 4:

Deuterium Enrichment by Proton Exchange Membrane Water Electrolysis with Electrolyte Circulation

4.1 Introduction

Consumption of fossil fuels and its negative impact on the environment has brought hydrogen energy to the forefront as a promising renewable source [1]. Recently, hydrogen isotopes have attracted attention as a new energy source. A reason for the increasing interest is that the isotopes, deuterium (D) and tritium (T), can be used in nuclear fusion [2, 3]. Corresponding research has been conducted since the early 1950s, and the National Ignition Facility in the United States recently achieved ignition for the first time [4]. Thus, the demand for separating and purifying hydrogen isotopes is increasing.

Corresponding separation technology has been studied since the 1930s [5, 6]. However, the physical and chemical properties of the isotopes are similar, which renders separation difficult. The major separation methods in industrial applications are cryogenic distillation (using the differences of equilibrium vapor pressure [7-9]), chemical exchange (using isotope exchange reactions between the liquid and gas phases [10-13]), water electrolysis (using the differences of equilibrium potential [14, 15]), as well as combined electrolysis and chemical exchange [16, 17].

The water electrolysis used for industrial purposes is alkaline [18-20]. The cathode and anode electrolyte are often separated by diaphragms that permeate hydroxide ions as well as water molecules. Alkaline water electrolysis has advantages of not using precious metals and easy operation; whereas it has drawbacks such as high risk of mixing hydrogen and oxygen through the diaphragm, high ohmic loss between the diaphragm and electrolyte, low current density (200–500 mA cm^{-2}), and inability to operate under high pressure—which renders it difficult to miniaturize. Therefore, solid polymer electrolytes have been developed [21, 22]. Proton exchange membrane water electrolysis

(PEMWE) has been well developed for high-current operation [23, 24]. Because the polymer is acidic, it is possible to electrolyze pure water.

Electrolytic isotope separation exhibits high performance. It concentrates D in the liquid and H in the gas phase. Zeng et al. electrolyzed ion-exchange water (D concentration, CD ~150 ppm) by PEM and observed a small D enrichment in the water discharged from the anode [25]. By changing the current density and temperature, the separation factor ranged from 2.64–3.40, indicating that the CD in the electrolyte increased at high current densities and low temperatures. A calculation model for CD supported the experimental data. The researchers proposed that CD increased exponentially with electrolysis time, and finally reached about 10,000 ppm. Akutsu–Suyama et al. developed a heavy water enrichment system, combining a four-cell stack PEMWE and a heat sink-type catalytic combustor [26]. They electrolyzed relatively high D electrolyte (93.1% D) and concentrated up to 99.3%. The separation factor, which evaluates the separation performance, was 3.6. Although many papers have investigated electrolysis at low or high D concentrations, the medium CD region has not been investigated well. To produce D_2O from an arbitrary CD solution, it is essential to confirm D enrichment over a wide range of CD. Therefore, the initial CD of the electrolyte in this study was set from 10–50 at.%. PEMWE was conducted by circulating the electrolyte, which produced highly concentrated D_2O.

4.2 Experimental

Figure 4.1 shows a schematic of the experimental setup. A JARI standard cell (FC Development, Japan) was used. The electrode area was 25 cm^2. Electrolyte was a Nafion (NRE-212) membrane. The catalyst of the anode and cathode was IrO2 (0.55 mg cm^{-2}) and Pt (0.55 mg cm^{-2}), respectively. The porous transport layer was a Pt-plated Ti mesh for the anode and carbon for the cathode. The separator had a serpentine channel with 1-mm depth and width. The channel was fabricated in a square area (5 cm × 5 cm). The electrolytic solution was pure water. CD (10, 30, and 50 at%) was adjusted by adding heavy water (99.9% D, Sigma–Aldrich, USA). Water was supplied to the cathode with a peristaltic pump (MasterFlex 07528-30, Cole–Parmer Instrument, USA). The flow rate was 2.1 mL min^{-1}. A DC power supply (PLZ164WA, Kikusui Electronics, Japan) was used and constant-current electrolysis (0.24 A cm^{-2}) was conducted. All experiments were performed under room temperature and atmospheric pressure.

Hydrogen gas from cathode was introduced into Q-mass (Qulee-HGM 202, Ulvac, Japan) after passing through a gas–liquid separator. The mass numbers 2 (H_2), 3 (HD), and 4 (D_2) were measured. The D separation was evaluated by calculating α. The value of α was obtained as follows,

$$\alpha = \frac{\frac{[\mathrm{H}]_{\mathrm{gas},t}}{[\mathrm{D}]_{\mathrm{gas},t}}}{\frac{[\mathrm{H}]_{\mathrm{liq},t}}{[\mathrm{D}]_{\mathrm{liq},t}}}, \tag{4.1}$$

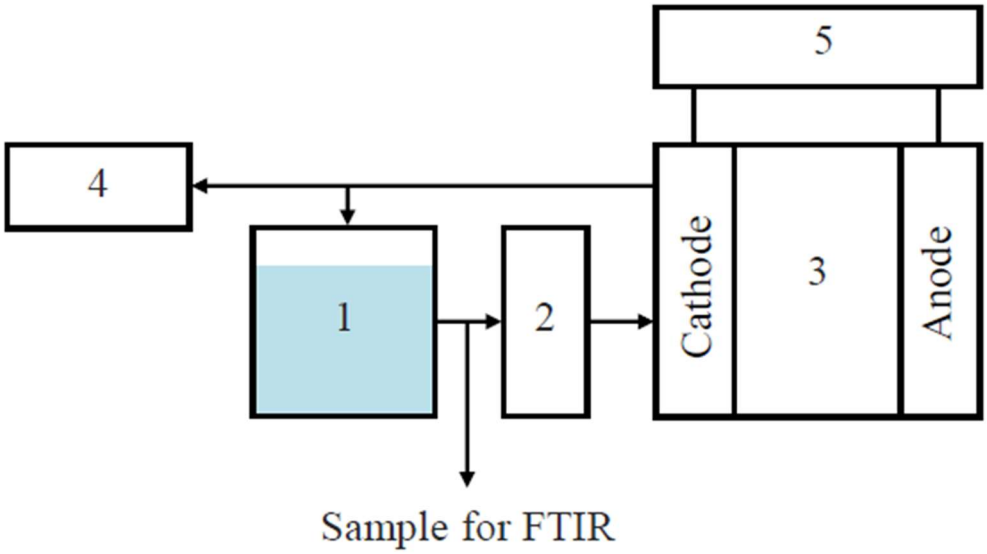

Figure 4.1 Schematic of experimental setup (1: Electrolyte in gas–liquid separator/reservoir, 2: Liquid feed pump, 3: PEM, 4: Q-Mass, 5: DC power supply).

where [H] and [D] represent the H and D atomic concentrations, respectively.

Nonelectrolyzed water was drained from the cell. It was passed to the gas–liquid separator and supplied to the cell again. When the electrolyte consumption ratio R was approximately 50%, 75%, 84%, and 88% to 93%, the CD was checked. A sample of the electrolyte was abstracted with a syringe. The sample was analyzed by attenuated total reflection–Fourier-transform infrared (ATR–FTIR) spectroscopy (FTIR-4200, JASCO International, Japan). FTIR measurements were performed in the range of 400–4000 cm^{-1} at a resolution of 2.0 cm^{-1} and an integration number of 100. Reference spectra were measured in air. The areas of the three peaks corresponding to the vibration bending modes of $A(D_2O)$ (1210 cm^{-1}), A(HDO) (1445 cm^{-1}), and $A(H_2O)$ (1645 cm^{-1}) were measured [27].

4.3 Calculation of D Mass Balance

The transient mass balance of H and D was expressed with the following equations, respectively,

$$\mathrm{H}: n_{\mathrm{H_2O},\,t+1} = n_{\mathrm{H_2O},\,t} - n_{\mathrm{H_2},\,t} \tag{4.2}$$

$$\mathrm{D}: n_{\mathrm{D_2O},\,t+1} = n_{\mathrm{D_2O},\,t} - n_{\mathrm{D_2},\,t}\ , \tag{4.3}$$

where $n_{\mathrm{x},\,\mathrm{t}}$ is the mole mass of component x at time t. For simplicity, HDO is not considered here.

Terms $n_{\mathrm{H2O},\ t}$ and $n_{\mathrm{D2O},\ t}$ were expressed with the following equations, respectively,

$$n_{\mathrm{H_2O,t}} = V_{\mathrm{ele},\,t} \times \rho_{\mathrm{ave},\,t} \times \frac{\left(100 - C_{\mathrm{D},\,t}\right)}{18} \tag{4.4}$$

$$n_{\mathrm{D_2O},\,t} = V_{\mathrm{ele},\,t} \times \rho_{\mathrm{ave},\,t} \times \frac{C_{\mathrm{D},\,t}}{20}, \tag{4.5}$$

where $V_{\mathrm{ele},\,t}$ (mL) is volume, $\rho_{\mathrm{ave},\,t}$ (g $\mathrm{mL^{-1}}$) is average density, and $C_{\mathrm{D},\,t}$ (%) is C_{D} of the electrolyte. The value of $\rho_{\mathrm{ave},\,t}$ was calculated from the density of H_2O (ρ_{H2O} = 0.9982 g $\mathrm{mL^{-1}}$), and D_2O (ρ_{D2O} = 1.107 g $\mathrm{mL^{-1}}$) as follows,

$$\rho_{\mathrm{ave},\,t} = \frac{\left(100 - C_{\mathrm{D},\,t}\right)}{100} \times \rho_{\mathrm{H_2O}} + \frac{C_{\mathrm{D},\,t}}{100} \times \rho_{\mathrm{D_2O}}\ . \tag{4.6}$$

Terms $n_{H2,\,t}$ and $n_{D2,\,t}$ were expressed with the following equations, respectively

$$n_{\mathrm{H_2},\,t} = \frac{\frac{[\mathrm{H}]_{\mathrm{gas},t}}{[\mathrm{D}]_{\mathrm{gas},t}}}{1 + \frac{[\mathrm{H}]_{\mathrm{gas},t}}{[\mathrm{D}]_{\mathrm{gas},t}}} \times n_{\mathrm{gas},t} \tag{4.7}$$

$$n_{\mathrm{D_2},\,t} = \frac{1}{1 + \frac{[\mathrm{H}]_{\mathrm{gas},t}}{[\mathrm{D}]_{\mathrm{gas},t}}} \times n_{\mathrm{gas},t}\,. \tag{4.8}$$

The total mole mass of evolved gas $n_{gas,\,t}$ was expressed by the electrolyte consumption rate v (mL min^{-1}),

$$n_{\mathrm{gas}} = v \times \rho_{\mathrm{ave},t} \times M_{\mathrm{ave},t}\,, \tag{4.9}$$

where M_{ave} (g mol^{-1}) is the average molecular weight of H_2O and D_2O, calculated as follows,

$$M_{\mathrm{ave},t} = \frac{100 - C_{\mathrm{D},t}}{100} \times 18 + \frac{C_{\mathrm{D},t}}{100} \times 20\,. \tag{4.10}$$

The H/D ratio in the gas $([H]/[D])_{gas,\,t}$ was obtained from the experimental value of α,

$$\frac{[\mathrm{H}]_{\mathrm{gas},t}}{[\mathrm{D}]_{\mathrm{gas},t}} = \alpha \times \frac{[\mathrm{H}]_{\mathrm{liq},t}}{[\mathrm{D}]_{\mathrm{liq},t}} = \alpha \times \frac{n_{\mathrm{H_2O},t}}{n_{\mathrm{D_2O},t}}. \tag{4.11}$$

Eq. 4.11 gives the values in Eqs. 4.4, 4.5, 4.7, and 4.8. Then, by subtracting Eq. 4.7 from Eq. 4.4, and Eq. 4.8 from Eq. 4.5, the mass quantity of the electrolyte at time t+1, $n_{H2O,}$

$_{t+1}$ and $n_{D2O,\ t+1,}$ was determined. The calculation was repeated until the electrolyte was completely consumed. For calculating C_D, the volumes of H_2O $V_{H2O,\ t}$ (mL) and D_2O $V_{D2O,\ t}$ (mL) were obtained as follows,

$$V_{H_2O,t} = n_{H_2O,t} \times 18 \times \rho_{ave,t} \tag{4.12}$$

$$V_{D_2O,t} = n_{D_2O,t} \times 20 \times \rho_{ave,t}. \tag{4.13}$$

Therefore, $C_{D,t}$ at t was expressed as follows,

$$C_{D,t} = \frac{V_{H_2O,t}}{V_{H_2O,t} + V_{D_2O,t}} \times 100\ . \tag{4.14}$$

4.4 Results and discussion

The electrolyte was circulated as a batch system and heavy water was produced. Constant-current electrolysis was performed from an initial electrolyte volume of 180 mL to approximately 10 mL for 83 h. The cell voltage was stable at about 1.9 V. Figure 4.2 shows the relationship between the electrolytic consumption ratio R and C_D. The following formula was used for calculating R,

$$R = \frac{V_{con}}{V_{int}}, \tag{4.15}$$

here V_{con} (mL) is the consumption volume of electrolyte and V_{int} (mL) is the initial volume before electrolysis. For reference, the electrolyte volume is shown on the upper X axis in Fig. 4.2. The value of C_D was calculated from FTIR data [27],

$$C_D = \frac{A(D_2O) + \frac{1}{2} A(HDO)}{A(H_2O) + A(D_2O) + A(HDO)} \tag{4.16}$$

where $A(x)$ is the area of component x obtained from the FTIR spectrum.

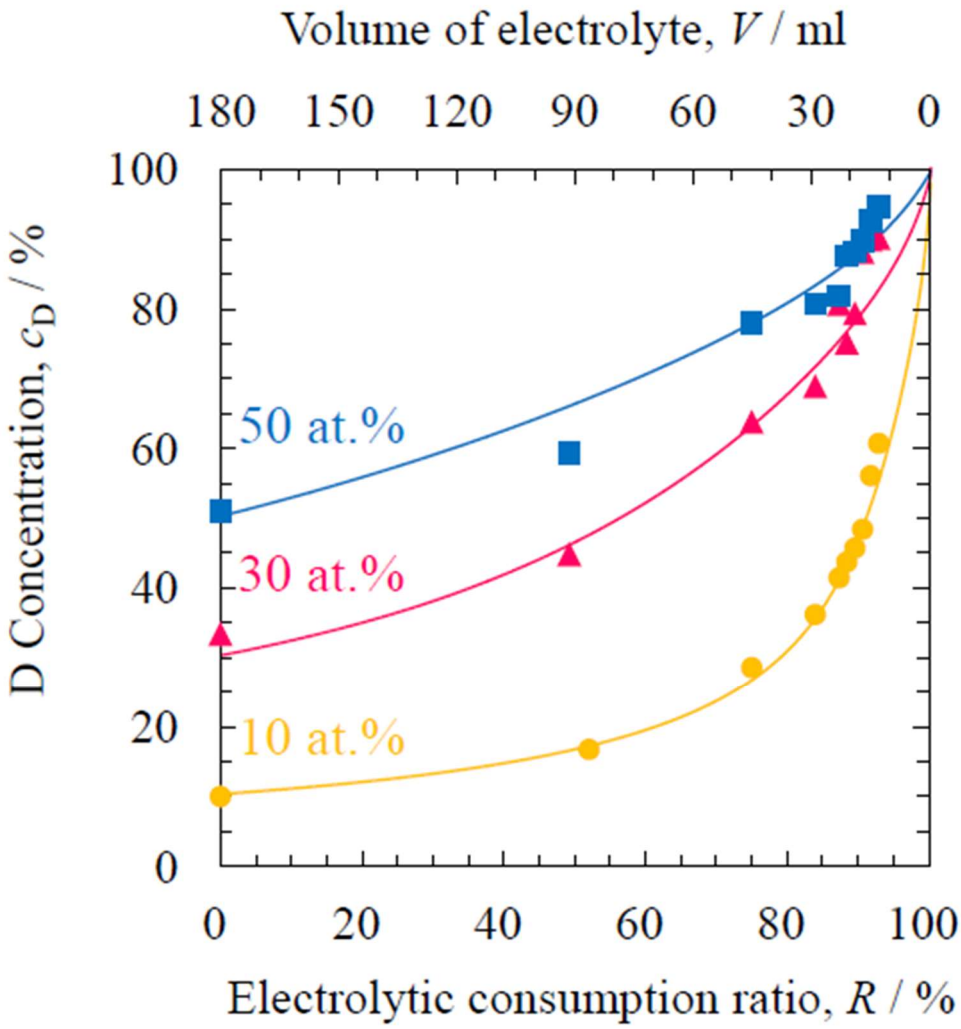

Figure 4.2 Dependency of D concentration on electrolytic consumption ratio during water electrolysis using 10 at.% D (circles), 30 at.% D (triangles), and 50 at.% D (squares) electrolyte.

For three electrolytes, C_D increased with increasing consumption. The batch method by PEMWE exhibited the same enrichment as the conventional alkaline method. The concentration variation at 10 at.% electrolyte was the largest, and C_D reached 60.7 at.%. At 50 at.%, C_D increased by approximately 1.8 times to 94.7 at.%. C_D changed negligibly until the water was consumed by about 40 % to 60 %. Thereafter, C_D ncreased exponentially as electrolysis continued. This is probably attributable to the mixture effect. A high C_D of the solution drained from the cell. When R was low, the drained water was mixed with a large quantity of nonelectrolyzed water in the reservoir, which averaged out C_D.

The solid line in Fig. 4.2 is the result from the mass balance described in Section 4.3. For all three solutions, the calculation agreed with the experimental plots. This suggests that the experimental results are valid in terms of the D mass balance between C_D and the water volume. However, when C_D increased, the experimental plots were higher than the theoretical plots for the 30 and 50 at% results. A reason for this result could be that the electrolyte was consumed faster than predicted, because the solution might evaporate over a long period of time.

The water consisted of three components: H_2O, HDO, and D_2O. When electrolysis was running, the solution in the reservoir was periodically sampled and analyzed by ATR–FTIR spectroscopy. In the experimental preparation, H_2O and D_2O were mixed to adjust the CD. The FTIR spectrum exhibited three distinct peaks: attributable to D_2O (1210 cm^{-1}), HDO (1445 cm^{-1}), and H_2O (1645 cm^{-1}). Therefore, there was formation of HDO as per the following chemical exchange reaction,

$$H_2O + D_2O \leftrightarrow 2HDO\,. \tag{4.17}$$

Interestingly, the relationship between R and the spectral peaks depended on the initial C_D . At 10 at%, the H_2O peak decreased and the HDO and D_2O peaks increased as *R* became higher. At 30 and 50 at%, the H_2O and HDO peaks decreased and the D_2O peak got larger with increasing *R*. To evaluate the percentage of H_2O, HDO, and D_2O in the water quantitatively, Fig. 4.3 shows the area ratio of each component relative to C_D. The area of the peaks in the FTIR spectra was used to calculate the ratio. The results at each initial C_D electrolyte are shown in different plots (circle: 10 at%, triangle: 30 at%, square: 50 at%). H_2O (unfilled plots) in the electrolyte decreased throughout the electrolysis. When C_D reached 70 at.%, the H_2O fraction was < 10%. In contrast, D_2O (filled plots) continued to increase until the end of electrolysis. The HDO fraction exhibited an upward convex peak with a maximum value at C_D = 50%.

The respective percentages depended on C_D of (1) ~30 at.%, (2) 30–50 at.%, (3) 50–70 at.%, and (4) ≥70 at.%. At (1), H_2O, HDO, and D_2O were abundant in this order. As C_D increased, H_2O decreased and HDO increased. D_2O also increased slightly. At (2), HDO exceeded H_2O in the order HDO, H_2O, and D_2O. At 50 at.%, HDO accounted for 50% of the solution, and H_2O as well as D_2O each occupied 25%. At (3), D_2O exceeded H_2O; and HDO, D_2O, as well as H_2O increased in that order. Afterward, H_2O decreased, D_2O increased, whereas HDO remained almost constant. At (4), H_2O was negligibly present. As C_D increased, HDO began to decrease. As the C_D increased, HDO began to decrease, whereas D_2O continued to increase. This change in the percentage of H_2O with C_D is consistent with the equilibrium state of H_2O, HDO, and D_2O in heavy water as revealed in a previous study [29]. Thus, each component in the electrolyte maintained the chemical equilibrium state of Eq. 4.17.

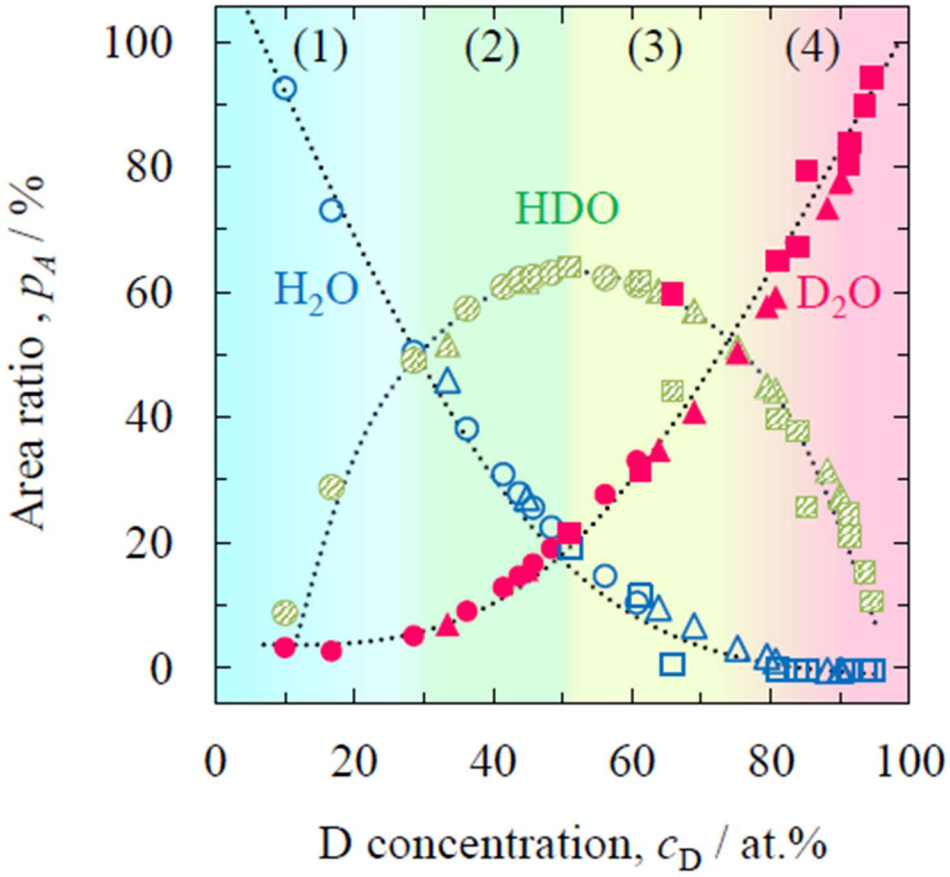

Figure 4.3 Area ratio of H_2O (unfilled), HDO (hatched), D_2O (filled) in liquid phase vs. D concentration (circle: 10 at%, triangle: 30 at%, square: 50 at%).

The components H_2, HD, and D_2 were present in the hydrogen gas. The gas was analyzed by Q-mass during electrolysis. Because constant-current electrolysis was performed, the time can be converted into electrolysis consumption. When the consumption ratio was small (R < 40%), the C_D variation was small (Fig. 4.2). Therefore, the ion current of each component did not change much. The components were initially in the order H_2, HD, and D_2. This result is similar to a previous study [28]. Thus, H was more concentrated in the gas. At high *R*, the ion current of D_2 increased substantially. However, the ion current of H_2 decreased symmetrically with that of D_2.

Figure 4.4 shows the ion current ratio of each gas component with C_D. Clearly, H_2 decreased and D_2 increased as C_D became higher. HD was a convex peak with a maximum at $C_D \approx 70$ at.%. The slope of the peak became steep at > 50 at.%. From Fig. 4.3, this might be attributable to the percentage of water molecules in the solution (or H/D ratio). When the C_D exceeded 50 at.% (H/D = 1), the percentage of H_2O present was less than that of D_2O. Hence, there was insufficient proton supply from the electrolyte. As a result, HDO and D_2O were electrolyzed. This led to a sharp decrease in H_2 and an increase in HD. At $C_D > 70$ at.%, HDO was < D_2O. Correspondingly, the HD fraction decreased. When D_2O was predominant at high C_D, a large volume of D_2 was generated. As a result, the following disproportionation reaction might have occurred,

$$H_2 + D_2 \leftrightarrow 2HD \qquad (4.18)$$

This probably contributed to the difference in the peak top position between HDO in Fig. 4.3 and HD in Fig. 4.4.

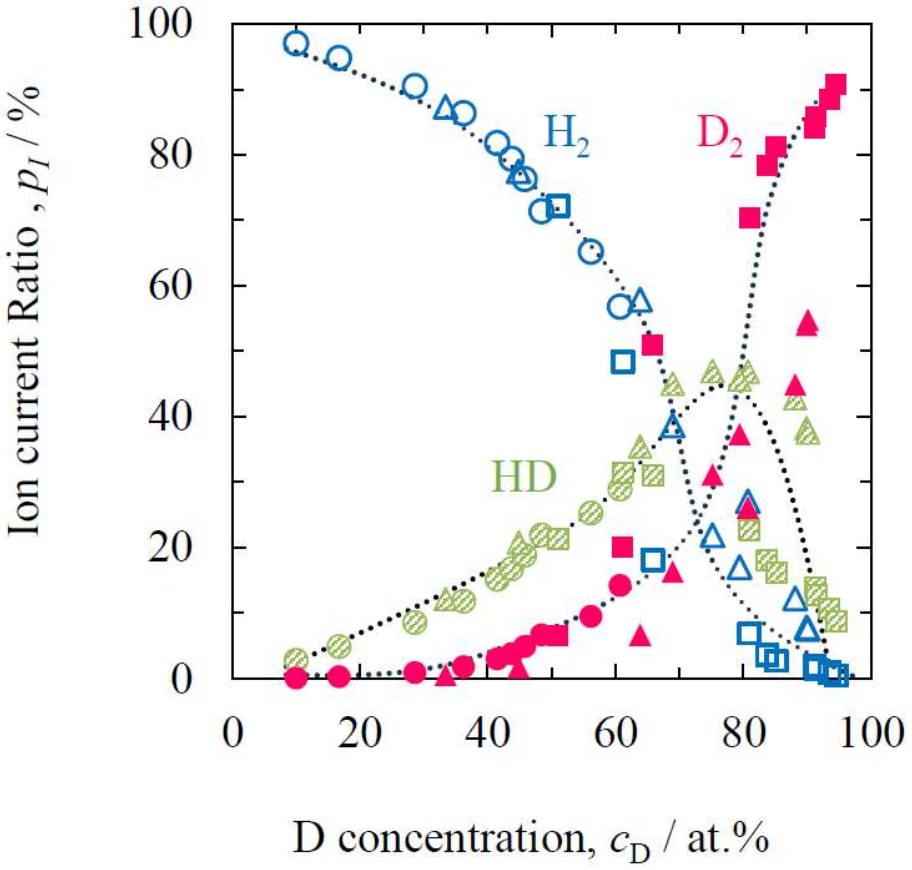

Figure 4.4 Ion current ratio of H_2 (unfilled), HD (hatched), D_2 (filled) in gas phase *vs.* D concentration in liquid phase (circle: 10 at%, triangle: 30 at%, square: 50 at%).

Figure 4.5 shows the dependence of α on C_D. The color gradation of the plot corresponds to the percentage of H_2O. An increase in the relative percentage of H_2O corresponds to a darker color. Term α was > 1 for all plots. H was concentrated in the gas and D in the liquid. Term α remained constant at ca. 4.0 from C_D = 10–30 at.%. This value is close to the separation factor of a previous study that also used Pt/C as a catalyst [30]. The constant α is attributable to the high content of H_2O (Fig. 4.3, in which H2O was the major component in solutions with low C_D). The separation performance was determined by the kinds of catalyst. When C_D was > 30 at.%, the H_2O concentration substantially decreased. This is attributable to the increase in HDO and D_2O. Under constant-current electrolysis, therefore, current was forced for D consumption. The result was to increase the CD of the gas, resulting in a lower α.

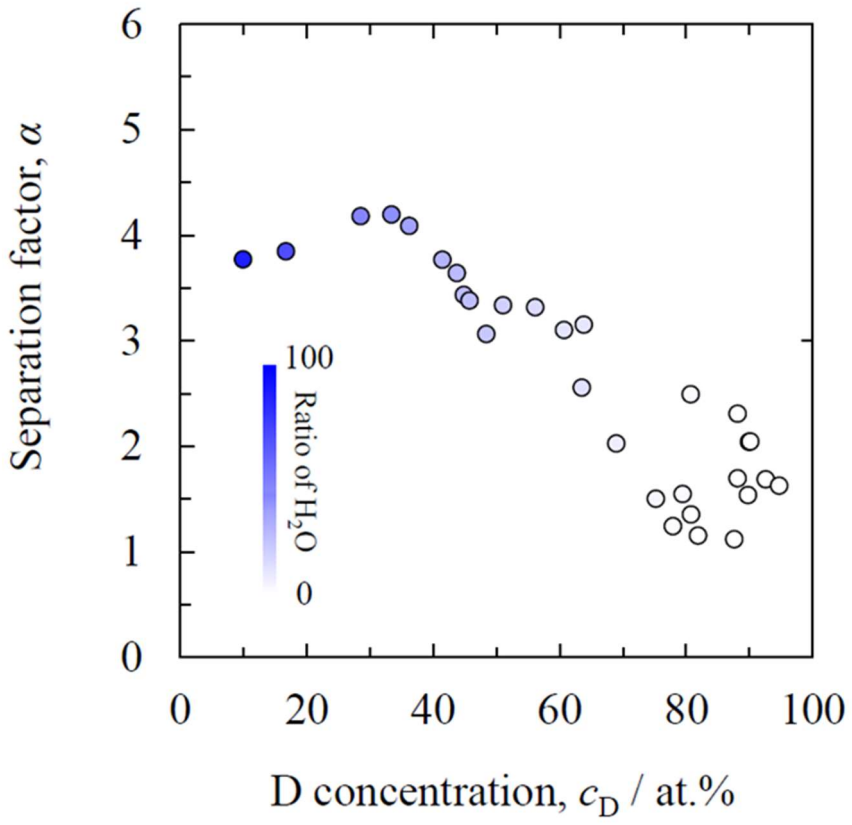

Figure 4.5 Separation factor α *vs.* D concentration in liquid phase.

4.5 Conclusions

In this experiment, PEMWE with a circulating electrolyte was carried out for producing heavy water. Three pure water containing 10, 30, and 50 at% D were prepared. When the electrolyte was consumed from 180 mL to 10 mL, the final C_D increased up to 61, 90, and 95 at%, respectively. The D enrichment was confirmed by a mass-balance model.

The FTIR results indicate that the electrolyte consisted of H_2O, HDO, and D_2O. The component ratio substantially depended on C_D. The major component was H_2O at < 30 at.%, HDO between 30 and 70 at.%, and D_2O at > 70 at.%. The factor α depended on the ratio of these components. The value of α was ca. 4.0 at C_D < 30 at%, whereas it decreased to ca. 1.5 in proportion to C_D. The poor separation at high C_D was probably attributable to decomposition of HDO and D_2O. This corresponded to the results of Q-Mass. When C_D was ca. 70 at.%, H_2 substantially decreased whereas HD and D_2 increased. The present results suggest that the electrolysis mode (constant-current or potential) depended on C_D. It was also important to consider disproportionation reactions for producing high-purity heavy water.

References

[1] S. C. Cowley, *Nature Physics*, **12**, 384 (2016).

[2] N. N. Gorelenkov, S. D. Pinches, K. Toi, *Nucl. Fusion*, **54**, 125001 (2014).

[3] J. Ongena, R. Koch, R. Wolf, H. Zohm, *Nature Physics*, **12**, 398 (2016).

[4] J. Tollefson, E. Gibney, *Nature*, **612**, 597 (2022).

[5] E. W. Washburn, H. C. Urey, *National Academy of Sciences*, **18**, 496 (1932).

[6] M. M. Ghoneim, S. Clouser, E. Yeager, *J. Electrochem. Soc.*, **132**, 1160 (1985).

[7] R. L. Combs, J. M. Googin, H. A. Smith, *J. Phys. Chem.*, **58**, 1000 (1954).

[8] D. Park, J. Jung Urm, J. Lee, M. H. Chang, J. M. Lee, *Int. J. Hydrog. Energy*, **46**, 24135, (2021).

[9] W. Ding, X. Fu, C. Chen, J. Wang, J. Hou, C. Xiao, H. Huang, H. Wang, *Sep. Purif. Technol.*, **324**, 12461 (2023).

[10] M. Mochizuki, S. Noda, T. Morishita, *Radioisotopes*, **36**, 163, (1987).

[11] Z. Lu, J. Li, X. Fu, J. Hou, G. Ran, C. Xiao, X. Wang, *Int. J. Hydrog. Energy*, **47**, 18080 (2022).

[12] L. Ye, D. Luo, T. Tang, W. Yang, P. Zhao, *Int. J. Hydrog. Energy*, **39**, 6604 (2014).

[13] S. Hu, J. Hou, L. Xiong, K. Weng, T. Yang, Y. Luo, *Sep. Purif. Technol.*, **77**, 214 (2011).

[14] D. L. Stojić, Š.S. Miljanić, T.D. Grozdić, D.D. Golobočanin, S.P. Sovili, M.M. Jakšić, *Int. J. Hydrog. Energy*, **19**, 587 (1994).

[15] X. Xue, M. Zhang, F. Wei, C. Liang, J. Liang, J. Li, W. Cheng, K. Deng, W. Liu, *Int. J. Hydrog. Energy*, **47**, 26842 (2022).

[16] T. Sugiyama, Y. Asakura, T. Uda, T. Shiozaki, Y. Enokida, I. Yamamoto, *Fusion Eng. Des.*, **81**, 833 (2006).

[17] Y. Sakharovski, V. Tkachenko, *J. Radioanal Nucl. Chem.*, **304**, 357 (2015).

[18] W. Kreuter, H. Hofmann, *Int. J. Hydrog. Energy*, **23**, 661 (1998).

[19] C. Daoudi, T. Bounahmidi, *Int. J. Hydrog. Energy*, in press.

[20] G. Gahleitner, *Int. J. Hydrog. Energy*, **38**, 2039 (2013).

[21] P. Millet, F. Andolfatto, R. Durand, *Int. J. Hydrog. Energy*, **21**, 87 (1996).

[22] M. Götz, J. Lefebvre, F. Mörs, A. M. Koch, F. Graf, S. Bajohr, R. Reimert, T. Kolb, *Renewable Energy*, **85**, 1371 (2016).

[23] M. Carmo, D. L. Fritz, J. Mergel, D. Stolten, *Int. J. Hydrog. Energy*, **38**, 4901 (2013).

[24] J. Hemauer, S. Rehfeldt, H. Klein, A. Peschel, *Int. J. Hydrogen Energy*, **48**, 25619 (2023).

[25] N. Zeng, C. Hu, C. Lv, A. Liu, L. Hu, Y. An, P. Li, M. Chen, X. Zhang, M. Wen, K. Chen, Y. Yao, J. Cai, *Sep. Purif. Technol.*, **310**, 123148 (2023).

[26] K. Akutsu-Suyama, H. Sajiki, M. Ueda, M. Asamotoc, Y. Tsutsumi, *RSC Adv.*, **12**, 24821 (2022).

[27] A. Pozio, S. Tosti, *Int. J. Hydrog. Energy*, **44**, 7544 (2019).

[28] K. Harada, R. Tanii, H. Matsushima, M. Ueda, K. Sato, T. Haneda, *Int. J. Hydrog. Energy*, **45**, 31389 (2020).

[29] J. Max, C. Chapados, *J. Chem. Phys.*, **116**, 4626 (2002).

[30] H. Matsushima, H. Sato, M. Ueda, and H. Ito, *J. Electrochem. Soc.*, **166**, F566 (2019).

Nomenclature

$A(D_2O)$	Area of D_2O obtained by FTIR
$A(HDO)$	Area of HDO obtained by FTIR
$A(H_2O)$	Area of H_2O obtained by FTIR
$C_{D,t}$	Concentration of D in the electrolyte at time *t* (at.%)
$[D]_{gas,t}$	Atomic concentration of D in the gas at time *t*
$[D]_{liq,t}$	Atomic concentration of D in the electrolyte at time *t*
$[H]_{gas,t}$	Atomic concentration of H in the gas at time *t*
$[H]_{liq,t}$	Atomic concentration of H in the electrolyte at time *t*
$M_{ave,t}$	Average molecular weight of H_2O and D_2O (g mol^{-1})
$n_{gas,t}$	Total mole mass of evolved gas at time *t* (mol)
$n_{D_2,t}$	Mole mass of component D_2 at time *t* (mol)
$n_{D_2O,t}$	Mole mass of component D_2O at time *t* (mol)
$n_{H_2,t}$	Mole mass of component H_2 at time *t* (mol)
$n_{H_2O,t}$	Mole mass of component H_2O at time *t* (mol)
R	Electrolytic consumption ratio (%)
$V_{ele,t}$	Volume of the electrolyte at time *t* (mL)
$V_{D_2O,t}$	Volume of D_2O (mL)

Chapter 5:

General Conclusion

In recent years, hydrogen has been used to reduce CO_2 emissions and as a substitute for fossil fuels to prevent global warming. Hydrogen has isotopes, deuterium and tritium, which differ in neutrons. Deuterium is used to extend the life of semiconductors and to increase the conversion efficiency to light in organic EL. Deuterium is also used in pharmaceuticals and optical fibers. Tritium is expected to be used as fuel in nuclear fusion. For these reasons, hydrogen isotope separation technology is needed. Hydrogen isotope separation technology is used to enrich deuterium from its natural abundance. And the technology is used to maintain the purity of deuterium in heavy water reactors, and to remove tritium discharged from fusion reactors.

In conventional method in hydrogen isotope separation, isotopes are generally separated according to their different physical properties. These methods includes gas-phase adsorption, cryogenic distillation, electrolysis, and water-hydrogen chemical exchange. Ideally, the separation method should require low energy and have a high separation factor to separate. The electrolytic method has the disadvantage of high energy consumption despite its high separation factor. For this reason, the CECE method is used in industry, which combines the electrolysis and water-hydrogen chemical exchange methods for separation. In this method, gas containing hydrogen isotopes generated by electrolysis is passed through the catalytic column for the water-hydrogen chemical exchange process. Although this method improves the separation factor compared to the method using only an electrolyzer, the energy consumption for gasification is still high, and a catalytic tower using platinum is required, making the cost and size of the equipment an issue.

To solve these problems, this study proposes a method using a fuel cell instead of a catalytic tower. This method is called the CEFC method. Electricity is recovered by

generating electricity in the fuel cell, enabling a reduction in energy consumption for gasification. The basic configuration of the system needs to be determined for the practical application of the CEFC method.

The humidification configuration in system must be determined because the humidification of the supplied gas is important to the performance and degradation of the fuel cell. In addition, as with the catalyst tower in the CECE method, the catalyst in the fuel cell is also made of platinum, so it is possible to perform VPCE and LPCE in water-hydrogen chemical exchange methods. Therefore, the effects of humidification on the separation process in a fuel cell and the effect of the gas-liquid ratio of water inside the fuel cell were investigated. In the electrolysis method, deuterium was concentrated in a batch process, and its validity as a separation method was verified. We also developed a mass balance equation and verified that the concentration process can be predicted by simulation.

In Chapter 1, various hydrogen isotope utilization and separation methods were discussed, including the CECE and CEFC methods. Additionally, the basic principles of fuel cells and electrolysis were explained, along with their potential for future development. The purpose of this study is clearly stated. In this research, the effect of water supplied to the fuel cell was investigated on the separation. The effects of water vapor and liquid water inside the fuel cell were also investigated. By clarify these principles, it is able to determine the humidification configuration of the fuel cell system for the practical application of the CEFC method.

In Chapter 2, we confirmed the effects of water vapor, oxygen, and power generation on hydrogen isotope separation by fuel cell. It was found that the separation can do by supplying humidified gas to the fuel cell. The separation factor was further

improved by power generation. Therefore, the synergistic effect of VPCE and electrochemical reaction in D separation was demonstrated. The mass balance of deuterium was also measured, and it was found that D does not stay inside the fuel cell and is correctly separated. With respect to whether the fuel cell generates electricity or not, it was found that the deuterium concentration in the generated water becomes thinner as a concentration. Although the deuterium concentration in the produced water is transferred in a larger volume of D when the fuel cell generates electricity.

In Chapter 3, the effect of humidification amount inside the fuel cell was examined. By examining the separation coefficient is affected by the difference in the amount of water vapor supplied and the vapor/liquid ratio of the water inside the fuel cell. We also constructed calculation model for the equilibrium conversion using equilibrium constants. And we compared the calculated values with experimental values. By increasing the amount of water supplied to the fuel cell, the separation factor could be improved. It was also found that condensation inside the fuel cell decreased the separation factor. The separation factor was calculated from the equilibrium conversion and compared with the experimental results, and it was found that the calculation did not agree with the results when condensation was allowed to occur. This suggests that the decrease in the amount of water vapor due to condensation and the decrease in the catalyst surface area due to the liquid water inhibited the separation.

In Chapter 4, concentration experiments were conducted using the electrolytic method to simulate the production of heavy water with different initial concentrations. In order to predict the concentration, calculation model based on mass balance was constructed and compared with the experiment. The calculated D concentration matched with the experimental D concentration, then calculation model was confirmed the validity.

The separation factor was found to vary with D concentration, and it was found to decrease with higher D concentration, which was attributed to the decomposition of HDO and D_2O.

List of Achievements

Papers

1. **"Effect of water vapor on deuterium separation by a polymer electrolyte fuel cell"**

   K. Furusawa, T. Nago, M. Ueda, H. Matsushima

   International Journal of Hydrogen Energy, **47**, 36248-36253 (2022).

2. **"Application of membrane electrode assembly for water hydrogen isotope exchange"**

   K. Furusawa, T. Nago, M. Ueda, H. Matsushima

   International Journal of Hydrogen Energy, **50**, 629-634(2024)

Conferences

1. **"Effect of Water Vapor on Hydrogen Isotopes Separation by Polymer Electrolyte Fuel Cell"**

   K. Furusawa, T. Nago, M. Ueda, H. Matsushima

   244th ECS Meeting, F02-1365, Gothenburg, Sweden, 2023 October.

2. **"Effects of Liquid and Vapor on Hydrogen Isotope Separation Using Fuel Cell"**

   K. Furusawa, T. Nago, I. Sato, M. Ueda, H. Matsushima

   Atomic Energy Society of Japan 2023 Fall Meeting, 2B05, Nagoya, Japan, 2023 September.

3. **"Highly Deuterium Concentration in Electrolyte by PEM Water Electrolysis"**

   I. Sato, K. Furusawa, H. Matsushima, M. Ueda

   Atomic Energy Society of Japan 2023 Fall Meeting, 2B06, Nagoya, Japan, 2023 September.

4. **"Effects of Water Vapor on Hydrogen Isotope Separation Using Fuel Cells"**

   K. Furusawa, T. Nago, H. Matsushima., M. Ueda

   The 89th ECSJ Spring Meeting, 3H07, Osaka, Japan, 2022 March.

Others

Paper

1. **"Effect of Anode Gas Circulation on Deuterium Isotope Separation by Polymer Electrolyte Fuel Cell"**

   T. Nago, K. Furusawa, M. Ueda, H. Matsushima

   International Journal of Hydrogen Energy, **50**, 1598-1603(2024)

Conferences

1. **"Deuterium Isotope Separation by Polymer Electrolyte Fuel Cell with Gas Circulation System"**

   T. Nago, K. Furusawa, M. Ueda, H. Matsushima

   244th ECS Meeting, F02-1366, Gothenburg, Sweden, 2023 October.

2. **"Study of Catalyst Loading for Deuterium Separation by PEFC**

   T. Nago, K. Furusawa, H. Matsushima, M. Ueda

   2022 ECSJ Fall Meeting, 1P14, Yokohama, Japan, 2022 September.

3. **"Effect of Anode Gas Circulation on Deuterium Separation in Fuel Cell"**

   T. Nago, K. Furusawa, H. Matsushima, M. Ueda

   The 89th ECSJ Spring Meeting, 1H11, Osaka, Japan, 2022 March.

Acknowledgments

In completing this research, I received support by many individuals. First of all, I express my deepest gratitude to my thesis supervisor Professor Dr. Hisayoshi Matsushima. His expertise and experience in isotope separation using fuel cell were invaluable in advising me on this research. He provided me with advice and support throughout the research process from the research plan to writing the paper. In particular, he assisted me in writing the paper and preparing it for publication. Despite my different field of specialization, he accepted me your laboratory member. Since joining the laboratory in 2021, you have provided valuable support for my activities.

I would like to express my immense gratitude to Professor Dr. Mikito Ueda for his exceptional guidance and invaluable advice throughout this research. I would like to extend my heartfelt thanks to Professor Dr. Shigehito Isobe and Dr. Seiichi Watanabe for many valuable suggestions and insightful feedback as reviewers of this research. Their suggestions have improved the quality of this research.

I would like to express my immense gratitude to my co-researcher, Mr. Toranosuke Nago. He assembled the experimental apparatus and conducted the experiments. We gained so many valuable insights through our discussions. In the chapter on water electrolysis, I would like to express my immense gratitude to my co-researcher, Ms. Ibuki Sato for her cooperation.

I am truly grateful to my family for their support and understanding in this research. They have been very understanding in terms of finances for tuition. Additionally, they recognized that I commuted to Hokkaido and provided me with support.

I would like to write some background on the completion of this research paper. Since 2019, I had been looking for new value-creating applications of the fuel cells. In this process, I found new value that is hydrogen isotope separation using fuel cells. I thought that this research could provide new value to society using the results of my research on fuel cells for automobiles. In 2020, I started the collaborative research project with Honda R&D. In the process, I decided to enter a doctoral program due to clarify my understanding of the fundamental phenomena in the separation process. Especially I would like to clarify the effects of water vapor and liquid water in fuel cells. Although it was difficult to work in a situation where many movements and activities were restricted by the effects of Covid-19. I believe that I was able to complete this thesis without giving up with the support of the many individuals mentioned.

I would like to conclude this doctor thesis with the belief that the results of this research will be value to mankind in the future.

February 2024

Koichiro Furusawa